FCTUC DEPARTAMENTO DE ENGENHARIA CIVIL
FACULDADE DE CIÊNCIAS E TECNOLOGIA
UNIVERSIDADE DE COIMBRA

Assessment of the behaviour of T-stub joint under impact loading

Master Course in Steel and Composite Construction

Author:

João Nuno Bregieiro Ribeiro

Scientific Supervision:

Professor Doctor Aldina Maria da Cruz Santiago

Professor Doctor Maria Constança Rigueiro

Coimbra, July 2014

Thesis submitted in partial fulfilment of the requirements for the degree of Master of Science in Steel and Composite Construction

· U C ·

Institute for Sustainability and

Innovation in Structural Engineering

ACKNOWLEDGMENTS

The author would like to thank the collaboration of Professors *Aldina Santiago* and *Constança Rigueiro* for their kind support and guidance, and his colleagues at the ISISE research institute for the motivation and friendship.

The work developed had the financial support from Ministério da Educação e da Ciência (Fundação para a Ciência e a Tecnologia) under research project *PTDC/ECM/110807/2009*.

ABSTRACT

Accidental loadings due to blast or impact may easily cause failure of the elements that are exposed or located in the vicinity of the hazard, leading in some cases, to the progressive collapse of part or even the whole structure. Assessment of the structural over strength is critical for structural engineers to ensure that arrest collapse mechanisms are developed and guarantee a certain level of safety. In steel frames the loss of a bearing element and the development of alternative unloading paths will take its toll on joints' strength and ductility.

The behaviour of joints subject to short transient loads is unsure and yet absent in current design guidelines; the present thesis addresses this issue by studying a validated finite element model and exploring analytical procedures to perform non-linear analysis of the T-stub model subject to impact loads. The models are validated against experimental results from the research project "ImpactFIRE", developed at the University of Coimbra. Welded T-stub with flange thicknesses of 10 and 15 mm (S335) bolted with M20's (8.8) are considered.

The T-stub model is used to describe the behaviour of components i) "column flange in bending" and ii) "end-plate in bending" present in a beam-to-column bending resistant connection. These components are responsible for the behaviour in the tension zone of joints, being able to provide ductility to a joint. The T-stub model is therefore a less complex model, when compared to a whole joint, yet it drives a joints' ductility capacity. Supplemented with a failure criterion describing the softening phase of the materials, the FE model captures the failure modes observed experimentally. Results show that the short transient loads applied induce elevated strain rates in the material enhancing its constitutive relationship, and therefore, enabling the T-stub to resist the maximum load observed in quasi-static cases with reduced displacement. Parametric studies show that stiffer T-stubs are less prone to develop elevated strain rates and therefore less keen to strength enhancement;

on the other hand, the ductility capacity is reduced for rather flexible T-stub (T-10) comparing the quasi-static and the short transient dynamic response.

The simplified approach established in the Eurocode to predict the resistance of T-stubs and a non-linear analytical model available in the literature, able to describe the post-limit regime, are improved to account for elevated strain rate effects. Once the non-linear routine is programed, it allows faster derivation of the response than building finite element models.

RESUMO

A ocorrência de acções acidentais de explosão ou de impacto podem facilmente causar a perda de capacidade resistente dos elementos estruturais situados na zona afectada, levando eventualmente ao colapso da estrutura. O desenvolvimento dos mecanismos de resistência ao colapso em pórticos metálicos sujeitos a acções acidentais requer ligações resistentes em flexão e capacidade de rotação suficiente para que se estabeleçam novos caminhos de descarga, pelo que a verificação da sobre resistência estrutural é fundamental.

O comportamento de ligações sob carregamentos de curta duração não se encontra ainda determinado nas normas de cálculo correntes, razão pela qual na presente tese se desenvolve um modelo de elementos finitos e se exploram modelos analíticos a estabelecer a resposta não linear de T-stubs. Os modelos são validados com resultados de ensaios experimentais desenvolvidos no âmbito do projecto de investigação "ImpactFIRE", desenvolvido na Universidade de Coimbra. São considerados T-stubs soldados chapas de espessura de 10 e 15 mm em aço S355, e aparafusados com M20 da classe 8.8. O modelo T-stub é escolhido por se tratar de um modelo simples mas que, no entanto, é responsável por descrever o comportamento de componentes responsáveis por fornecer ductilidade a uma ligação, nomeadamente o i) "banzo de coluna em flexão" e ii) "chapa de extremidade em flexão" do "método das componentes" para o cálculo de ligações. O modelo numérico desenvolvido inclui ao nível do material a descrição do comportamento na fase de amolecimento permitindo a captura dos modos de rotura observados experimentalmente. Verifica-se que carregamentos de curta duração induzem taxas de deformação elevadas no material capaz de alterar a lei constitutiva do material, incrementando a tensão de cedência e última do material, possibilitando que os T-stub resistam a carregamentos equivalentes ao máximo observado sob condições quasi-estáticas sem colapso e com um nível de deformação reduzido. Os estudos paramétricos levados a cabo mostram que T-stub mais rígidos sofrem

menos destes efeitos, mas que T-stubs mais flexíveis (T-10) podem ver a sua ductilidade reduzida quando submetidos a carregamentos de impacto.

A metodologia estabelecida nos Eurocódigos para o cálculo da resistência de T-stubs e um modelo não-linear disponível na literatura, capaz de descrever o comportamento pós-limite, são ajustados de forma a tomar em conta os efeitos de taxas de deformação elevada. Uma vez a sua rotina seja programada, o modelo não-linear permite obter a resposta de forma mais rápida do que construindo de um modelo de elementos finitos.

NOTATION

General (Ordered according to appearance)

t_f	Flange or plate thickness
l_{eff}	Total effective length of an equivalent T-stub
F	Force
$F_{T,i,Rd}$	Design resistance for each T-stub mode
$M_{pl,Rd}$	Resistance of the formed plastic hinges
$F_{t,Rd}$	Bolt's tension resistance
m	Bolt distance to the weld
n	Minimum bolt distance to a free edge
f_y	Yield strength
f_u	Ultimate strength
f_{ub}	Bolt ultimate strength
A_s	Tensile area of a bolt
k_2	Bolt strength reduction factor
K	Stiffness
k	Relative dimension of the plastic hinge length to the plate thickness
E	Elastic modulus
E_t	Tangent modulus
E_u	Ultimate modulus
A	Quasi-static yield strength
B	Strain hardening parameter
n	Strain hardening parameter
C	Strain rate constant
L	Characteristic length of the finite element

D	Damage scalar variable
L_0	Initial gauge length
$\bar{u}^{pl}$	Effective plastic displacement
K	Stiffness matrix
u	Vector of unknown displacements
F	External force vector
W	Work
M	Element mass matrix
C	Viscous damping
$u, \dot{u}, \ddot{u}$	Displacement and its first and second derivatives, velocity and acceleration
f	Frequency, $f = 1/\tau$
a_w	Weld throat thickness

Greek letters (Ordered according to appearance)

γ_{Mi}	Partial safety factor used for applied design situations
δ	Displacement
ε_y	Elastic strain
ε_u	Ultimate strain
$\dot{\varepsilon}$	Strain rate
σ_{eng}	Engineering stress
ε_{true}	Logarithmic plastic strain
σ_{dyn}	Dynamic stress flow
σ_{static}	Quasi-static stress flow
$\dot{\varepsilon_0}$	Quasi-static reference strain rate
$\dot{\varepsilon}^*$	Reference dimensionless plastic strain rate
σ_y	Yield strength
$\bar{\varepsilon}_0^{pl}$	Equivalent plastic strain at the onset of damage
$\bar{\varepsilon}_f^{pl}$	Equivalent plastic strain at failure
σ_H	Hydrostatic pressure stress
σ_{eq}	Equivalent Von Mises stress

α, β, γ	HHT algorithm parameters
τ	Period
Δ_t	Time-increment

Acronyms (alphabetic order)

DIF	Dynamic increase factor
ER	Strain rate
HHT	Hilber-Hughes-Taylor direct integration method
MISES	Von Mises stresses
PEEQ	Equivalent plastic strain
PH	Plastic hinge
SDEG	Damage scalar variable
SHBT	Split Hopkinson Bar test
TSWA	Top and seat with web angles

General steel material properties (Szuladziński, 2010):

Material	E GPa	ρ kg/m3	υ	G GPa	c_0 m/s	c_s m/s	E_{ef} GPa	c_p m/s
Steel	200	7850	0.3	76.92	5047.5	3130.4	269.23	5856.4

Where:

c_0	Uniaxial wave in thin bar
c_s	Shear wave, beam or medium
c_p	Pressure wave, confined bar or medium

CONTENTS

LIST OF FIGURES

LIST OF TABLES

PART I

INTRODUCTION

LITERATURE REVIEW

MATERIAL CHARACTERIZATION

FINITE ELEMENT MODEL

1. INTRODUCTION

A. Background & Context

The use of steel for structural purposes prompted the construction industry to go beyond and explore demanding structural shapes. Steel is a ductile, stiff and with a high resistant to weight ratio material; these properties allow for the production of moderately weighted structural elements able to perform in long spans. The use of steel for structural purposes is adequate for the pre-fabrication of elements (beams and columns) which, in turn, allows for a reduction of the construction time, on-site labour, and waste. Moreover, steel is fully reusable and recyclable, meaning that a structure can be disassembled and erected in a new location without losing its properties, or that its material can be used to cast new steel profiles.

Looking forward to higher pre-fabrication levels, the use of bolted steel joints to connect steel elements has soon evolved – Figure 1.1, avoiding welds forming a permanent connection between structural elements.

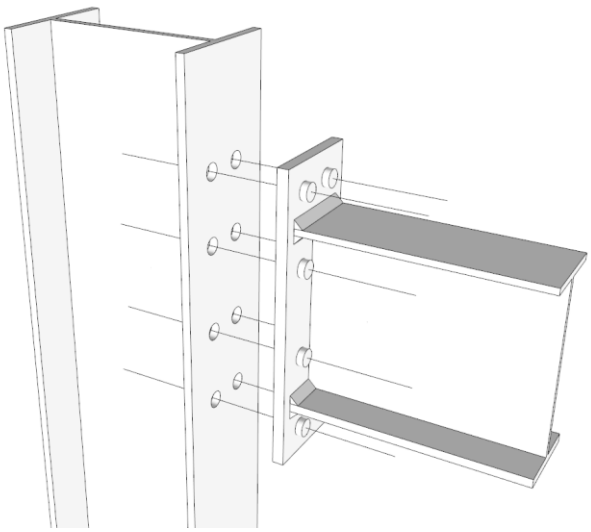

Figure 1.1 – Bolted beam to column joint

The use of bolted steel joints does not form a permanent bond between the structural elements and in turn allows for higher erection speeds and simpler assembly process; however, bolted steel joints usually require higher material quantities and preparation (geometry and connecting elements), whilst in-shop welding of connecting elements is unavoidable. Prefabrication control and requirements are tighter to ensure errors are kept to a minimum and financial turnover in comparison to on-site welding is achieved.

Despite any differences in the construction costs, welded and bolted steel joints in framed structures do not behave in the same way: welding material deposits often have higher resistance than the structural elements its connecting, therefore the connection can be usually assumed as rigid and with full resistance in what concerns common design situations. In the case of bolted joints, the introduction of additional connecting elements (such as an end-plate and bolts) requires increased verification, while a weakened structural point may be created. In order to keep the required amount of in-shop work to a reasonable level, bolted steel joints are often built and calculated as semi-rigid and with partial strength – Figure 1.2; this means that the joint's resistance may be weaker than the beam's plastic resistance and that the joint's rotational stiffness will condition the beam's support restriction, which in turn, will influence the beam's bending moment, deflection and also the frame's lateral stiffness.

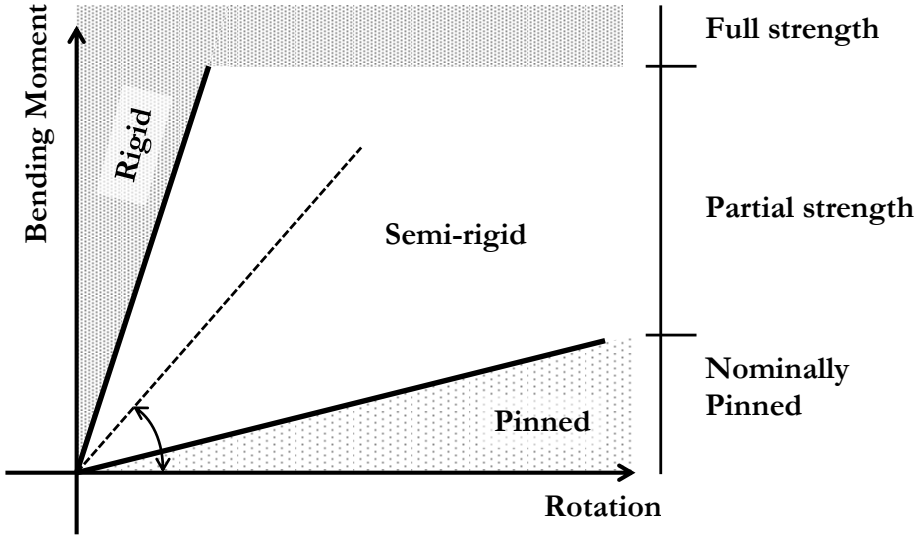

Figure 1.2 – Strength and stiffness of steel joints

Based on the research developed in the past decades, current European design guidance establishes joint categorization according to its stiffness, resistance and ductility, and takes advantage of using semi-rigid joints; once a commitment between a frame's lateral stiffness

and its joints stiffness is met, the use of semi-rigid joints can provide the structure with means of dissipating energy and develop deformations without fracture, while keeping construction costs at a reduced level. High ductility and energy dissipation is a matter well studied regarding the seismic behaviour of steel structures and guidance is provided in the Eurocodes (part 8) to perform a safe design.

The current Master Thesis focuses on the behaviour of bolted steel joint's under impact loading; when subject to rapidly applied loads, a joint's ductility may be reduced and compromise the structural ability to maintain its integrity. The lack of guidance on how joints behave under such loading conditions caught the attention of the research community to this theme. The objective is to understand and improve structural robustness to minimise the damage to people and property under extreme events, either accidental or terrorist driven. Current codes do provide rather empiric prescriptive rules to maintain integrity, but establishing the structural ability to develop alternative unloading paths depending on the joint's behaviour is yet an arduous task.

In addition, when subject to rapidly applied loads, elevated strain rates ought to be developed in the material; like most materials, mild steel's visco-plastic behaviour increases its strength when subject to strain rates higher than the quasi-static rate used to perform the material characterization generally required to design steel structures and joints. In what bolted steel joints is concerned, such event may increase the ratio of plate/bolt strength which in turn reduces its ductility; also, when subject to impact loading regimes, steel's toughness can be reduced leading to early fracture of the connecting elements (end-plate or bolt).

Looking forward to understand the extent of such behaviour, the Portuguese Foundation for Science and Technology (FCT – Fundação para a Ciência e a Tecnologia) provided financial support to the research project "ImpactFIRE". The project focuses on the design of robust steel joints capable of withstanding accidental impulsive loading which may arise mainly from impact and explosions, with special attention on the combined scenario of fire after impulsive loading. The topic has been addressed in the strategic research agenda of the European Steel Technology Platforms following public demands for improved safety in the in the design, manufacture and performance of steel structures, especially against natural hazards and accidental loading.

B. Objectives

Performance of steel joints under natural hazards and accidental loading remains a somewhat unclear theme; integrated within the framework of the research project "ImpactFIRE", the present thesis aims at the enhancement of the knowledge of the behaviour of steel joints under impact loading. Currenty, guidance for the design of steel joints is supplied by the Eurocode 3 –Part 1.8 – Design of Steel Joints; there, the behaviour of steel joints is obtained following the "component method", in which steel joints are discretized in its active components. Once each active component has been assembled in a spring model, the elastic behaviour and plastic resistance can be calculated. The T-stub model is used to establish the behaviour of components in the tension zone of bending resistant joints, namely the "column flange in bending" and the "end-plate in bending"; these two are often accountable for providing and limiting the stiffness and ductility of a joint.

In this way, the T-stub model remains a small and simple model, and yet it will drive the behaviour and provide ductility to a joint. Hence, the present thesis addresses the behaviour of the T-stub model under impact loading by establishing a validated finite element model able to describe its non-linear behaviour under rapidly applied loads and improvements in available analytical models. The finite element model is validated with data collected from the aforementioned research project "ImpactFIRE": the finite element model is firstly verified to be able to reproduce the behaviour of the T-stub under quasi-static loading; secondly it is extended to provide the response under impact loading. Once the numerical model is verified, a series of parametric studies are conducted identifying relevant parameters driving the behaviour and an effort to include elevated strain rate dependency on analytical models is undertaken.

Achievement of these main objectives requires building knowledge around finite element solutions, material characterization and it's modelling; during the thesis attention is given to the tools used to perform the transient non-linear dynamic analysis, building the elevated strain rate dependency and the application of a failure criterion enabling the prediction of the ultimate failure of the modelled specimens.

C. Thesis outline

The thesis is outlined in two different parts: Part I runs up to Chapter 4 (inclusive) presenting background on the object of study and its straight relation to research project "ImpactFIRE"; the characterization of the material properties and acknowledgement of the finite element method fundamentals for the development of advanced dynamic non-linear finite element analysis. Description of the finite element model developed is presented also presented in Part I whilst Part II presents its validation to static and short transient dynamic loads, discussion of the results from the parametric studies conducted and proposals for improvements in an analytical model available in the literature. Part I is delivered for fulfilment of lecture *Dissertation I* and Part II for fulfilment of *Dissertation II* from MSc in Steel and Composite Construction.

The current chapter is of introductory character, presenting the background & context of the matter in hand and the thesis objectives. A short presentation of the candidate, scientific supervision and host institution are also provided.

Chapter 2 presents the relevant state of the art regarding the design of steel joints subject to static and dynamic loads, particularly on authors working in development of analytical models establishing the T-stub non-linear response, studying joints under impact and blast loads and development of finite element models.

Chapter 3 introduces the relevant material properties required to perform non-linear analysis of T-stub under impact loads. Material characterization for later use in the numerical model including the viscoplastic characterization with data gathered from "ImpactFIRE" research project, and the damage behaviour modelling are presented

Chapter 4 concerns the basic principles required to perform analysis with the finite element method. Particularly, the solution algorithm and finite element selection are explored and the contact algorithm and von Mises yield criterion presented. This chapter regards the description of the finite element model built focusing on the assumed simplifications based on the geometry of the structural model and tested specimens, as well as the material input and dynamic properties of the finite element model.

Chapter 5 presents validation of the FE model for static and dynamic conditions against experimental results from "ImpactFIRE". Afterwards the effects of different load

application times and peak load are explored in a parametric study; the dynamic effects in T-stubs with flange thicknesses ranging from $t_f = 8$ to $t_f = 40$ mm are verified.

Chapter 6 explores a simplified analytical model (Eurocode 3, Part 1.8) and a non-linear analytical model available in the literature to describe the behaviour of T-stubs. The model is verified against previous static analysis and experimental results, whilst proposals to improve the model to describe dynamic loading conditions are made and compared previous results.

Chapter 7 presents the conclusions of the developed work and its findings, and future work suggestions.

D. Candidate presentation, scientific supervision and host institution

Candidate presentation:

João Ribeiro concluded his Bolonha Master's in Civil Engineering at the University of Coimbra in Sep. 2009 and joined Martifer Metallic Construction group where he worked as a structural designer. Since Feb. 2012 he has joined ISISE research group for the development of numerical analysis for the project "ImpactFIRE" and is currently finishing his MSc in Steel and Composite Construction.

Scientific supervision:

Aldina Santiago is Assistant Professor at the Civil Engineering Department of the University of Coimbra, in Portugal. She is involved in experimental research and coordination and teaching of steel related courses in the MSc and PhD programmes. She is a member of the Technical Committee TC10, and of the COST Action TU0904 (Application of Structural Fire Design). She has authored over 100 scientific papers in the field of exceptional loadings and steel structures.

Constança Rigueiro is Adjunct Professor at Polytechnic Institute of Castelo Branco and Invited Assistant Professor at the Civil Engineering Department of the University of Coimbra in Portugal where she is involved in the MSc and PhD programmes of Steel and Composite Construction. She has been working on dynamic behaviour of structures and in sustainable construction. In these subjects is author and co-author of 50 scientific papers.

Host institution:

The thesis is presented for fulfilment of the Master Course in Steel and Composite Construction provided by research group *ISISE – Institute for Sustainability and Innovation in Structural Engineering* (http://isise/smct/site/) held in the Civil Engineering Department of the University of Coimbra.

2. LITERATURE REVIEW

2.1 Introduction

Public awareness, fear and demand for safety measures have risen dramatically in the last decades. Modern terrorism is seen as the main cause, for targeting people's working and living places (World Trade Center, New York, 2001), but there are also accidental situations such as, accidental explosions, fire, or earthquakes that may endanger structures. Examples of these accidental hazards effects are portrayed in Figure 2.1.

a) 1948, Fukui – Earthquake.

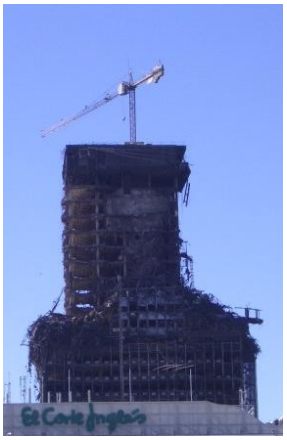

b) 2005, Windsor Tower, Madrid – Fire.

c) 1968, Ronan point, London – accidental gas explosion.

Figure 2.1 – Damaged structure under accidental hazards: a) earthquake; b) fire; c) accidental explosion.

The case depicted in Figure 2.1 c) was caused by an explosion in a kitchen on the 18th floor (approx. half height of the building) causing the failure of the edge precast walls required for load bearing. As the cladding was unable to redistribute gravitational loads from the structure above, the whole corner *progressively collapsed* as consecutive floors piled on top of each other. This event would eventually lead to the first approach for structures to be designed for notional column or beam removal, and minimum horizontal and vertical tying

provisions, delivered by the UK Building Regulation, in 1970, (Cormie & Smith, 2009). The main goal is to avoid the *disproportionate collapse* of buildings (as observed), by providing protective measures that can sustain the damage to its original zone of influence.

Joint behaviour is considered crucial to fully assess the structural stability in avoiding progressive collapse (McAllister, 2002) (Arup, 2011) (Ellingwood, 2007), (Cormie & Smith, 2009). Despite real evidences (see FEMA's report (McAllister, 2002)) and recent studies have highlighted joints as a critical component limiting structural frame's ductility and deformability, current design standards only provide information on its stiffness and resistance under quasi-static loading, available in Eurocode 3, Part 1.8 (EN 1993-1-8, 2005).

Regarding a whole building response, the EN 1991-1-7 (EN 1991-1-7, 2006) introduces two different approaches to avoid or control the consequences of accidental scenarios: i) strategies based on identification of the accidental actions, as internal explosions and impact (from road vehicles; forklift trucks; trains; ships and helicopters on roofs) where the accidental actions are represented by an equivalent static force corresponding to the equivalent action affects in the structure requiring strain rate effects to be considered on the description of the material properties of both the impactor and the structure; and ii) strategies based on limiting the extension of localized failure. These design strategies should be adapted to the consequences class classification of the structure according to the Annex B of the EN 1990; for highly categorised building a "*tie-force-based design*" is recommended to avoid disproportionate collapse. Further design approaches are described in (Cormie & Smith, 2009) namely the "*key element design*", where a limited number of elements are required to withstand a given abnormal load and the "*alternate path method*" in which structural ability to provide alternative load paths and load redistribution are addressed.

2.2 Theoretical approach to evaluate the non-linear response of the T-stub

The evaluation of the real behaviour of steel joint (Figure 2.2) is complex and requires the proper consideration of multi-phenomena namely the material's non-linearity (plasticity and strain hardening), geometrical non-linearity (local instability), non-linear contact behaviour between elements and residual stress conditions (Simões da Silva, 2008). Since the 1970's a considerable effort has been done studying the behaviour of steel joints. In the beginning, researchers were focused on the resistance and on the stiffness characteristics ((Zoetemeijer,

1974), (Jaspart, 1991), (Swanson & Leon, 2002)) leading, for example, to the "component method" established in EN 1993-1-8 (EN 1993-1-8, 2005). Thereafter the research emphasis has been on the evaluation of the joint ductility ((Simões da Silva *et al.*, 2002), (Girão Coelho & Simões da Silva, 2004)).

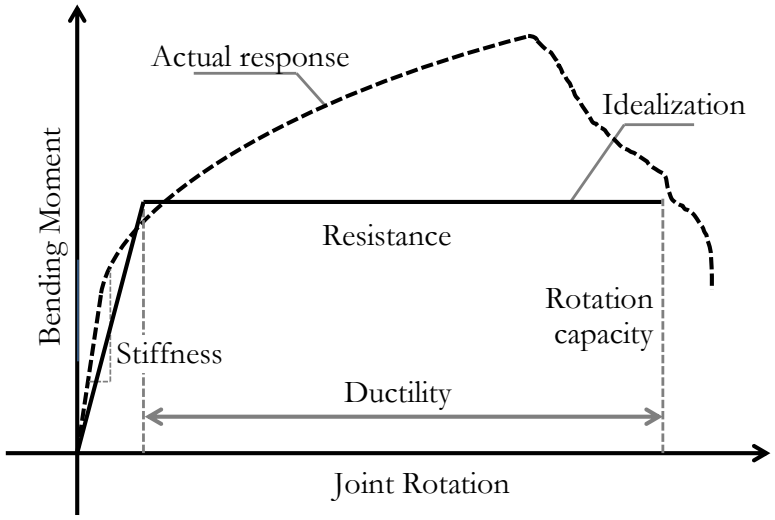

Figure 2.2 – Moment-rotation response of a joint

The component method requires the accurate characterization (stiffness, resistance and ductility) of each active component. These components represent a specific part of a joint that makes an identified contribution to one or more of the structural properties. The EN 1993-1-8 (EN 1993-1-8, 2005) specifies strength and stiffness properties for different components that allow the calculation of a wide range of beam-to-column, beam-to-beam and column base joint typologies.

The main active components in a beam-to-column bolted joint are: i) column web panel in shear; ii) column web in compression iii) column web in tension; iv) column flange in bending; v) end-plate in bending; vi) beam flange and web in compression; vii) beam web in tension and viii) bolts in tension, as shown in Figure 2.3. The T-stub model is used to evaluate the behaviour of components iv) and v), being them the main components that assure the joint ductility due to its high deformation capacity.

A T-stub is referred as a partial T-shaped section located in the joint's tension zone, as shown in Figure 2.4.

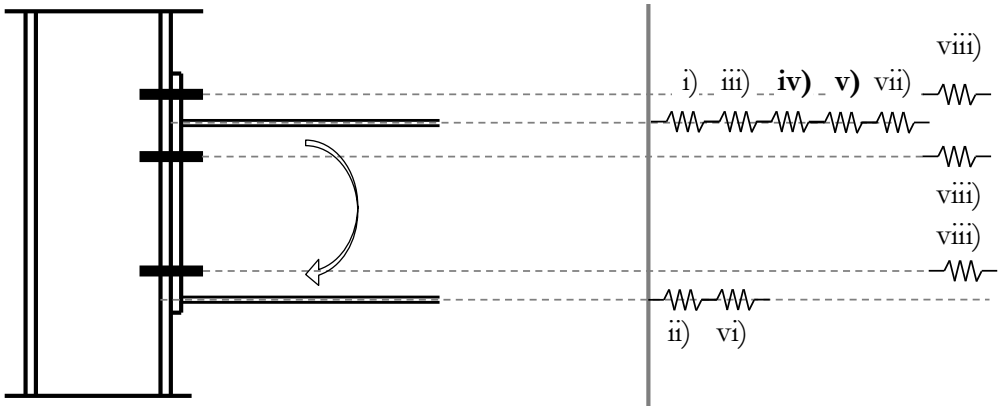

Figure 2.3 - Component method illustration.

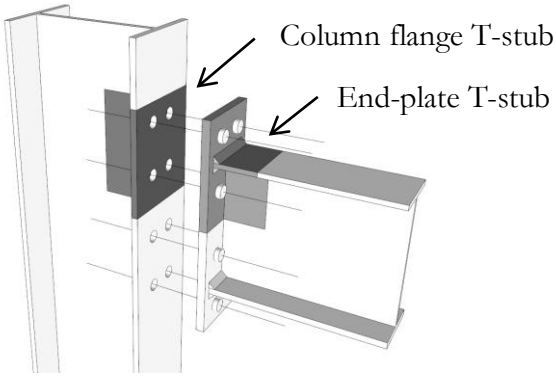

Figure 2.4 – "T-stub" section in a joint.

The formulation to calculate the plastic resistance of a T-stub according to Eurocode 3, Part 1.8 (EN 1993-1-8, 2005) is presented in equations (1) to (5). The first three equations describe each of the plastic failure modes illustrated in Figure 2.5; for *Mode Type 1*, two plastic hinges per flange leg are developed with the complete yielding of the flange (or plate): one at the bolt axis due to the bending moment induced by the prying forces and another next to the weld toe; for *Mode Type 2*, one plastic hinge per flange leg is developed before the failure of the bolts; while for plastic *Mode Type 3*, no plastic hinges are developed, being the plastic resistance limited by the bolt's strength. A T-stub's plastic resistance is, therefore, the minimum value obtained from them.

Equation (4) provides calculation for the resistance of the formed plastic hinges; it requires the consideration of the smallest yield line pattern (l_{eff}), commonly referred to as the effective width. Equation (5) provides the design tension resistance of a bolt. According to the Eurocode 3, Part 1.8, the yield line pattern may be described by means of *circular*, *non-circular* or even *beam* patterns; indeed, the minimum yield line pattern will enforce the smallest resistance and therefore should be considered for the calculation.

Concerning the stiffness, Eurocode 3, Part 1.8 (EN 1993-1-8, 2005) provides estimation of the elastic stiffness for T-stubs based on the same principle (definition of an effective width); once the elastic stiffnesses for each of the acting components are assembled into the spring model, a description of a joint's elastic stiffness can be obtained. A joints' typical moment-rotation response and Eurocode's prediction are described in Figure 2.2.

Mode Type 1: $$F_{T,1,Rd} = \frac{4.M_{pl,Rd}}{m} \quad (1)$$

Mode Type 2: $$F_{T,2,Rd} = \frac{2.M_{pl,Rd} + n\sum F_{t,Rd}}{m+n} \quad (2)$$

Mode Type 3: $$F_{T,3,Rd} = \sum F_{t,Rd} \quad (3)$$

In which:

$$M_{pl,Rd} = {}^{1}/_{4} \sum l_{eff}.t_f{}^{2}.f_y/\gamma_{M0} \quad (4)$$

and

$$F_{t,Rd} = \frac{k_2 f_{ub} A_s}{\gamma_{M2}} \quad (5)$$

Where $F_{T,i,Rd}$ is the design resistance for each T-stub mode; $M_{pl,Rd}$ the resistance of the formed plastic hinges based on the flange's geometric properties: l_{eff} and t_f, which are the total effective length of an equivalent T-stub and the flange thickness respectively; m and n are the bolt distance to the weld and the minimum bolt distance to a free edge; $F_{t,Rd}$ is a bolt's tension resistance; A_s is the tensile area of a bolt; k_2 is a factor taken with a value of 0.9 for bolts other than countersunk bolts (EN 1993-1-8, 2005); f_y and f_u are the yield and ultimate strengths (f_{ub} ultimate strength for the bolt), respectively and γ_{Mi} are partial safety factor used for applied design situations.

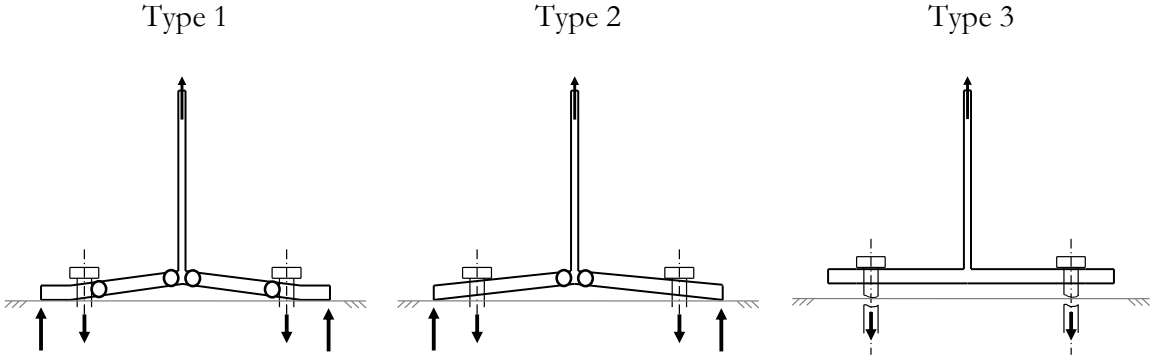

Figure 2.5 – T-stub plastic modes

Faella and co-authors (Faella *et. al.,* 2000) have developed an analytical procedure to evaluate the force-displacement curve of a T-stub until failure. It considers the three possible failure modes, as established in Eurocode 3, Part 1.8 (EN 1993-1-8, 2005), and thereafter calculates the ultimate rotation of each of the plastic hinges involved in the collapse mechanism. This approach is able to establish the force-displacement response through the integration of the curvature diagrams of each plastic hinge, up to failure of either the flange or the bolt, provided that a failure criterion is defined. Due to the closed form formulation, the authors are able to derive the force-displacement response of T-stub's by calculating the force and displacement for each of the four characteristic points used to establish the material's description (Figure 2.6a)). Additionally, the following approximations are reported: i) the approach is based on a 2D model (3D effects are not accounted for); ii) geometrical nonlinearity is disregarded; iii) compatibility between bolt and flange displacements is not considered; iv) the bolt material description is neglected due to its poor ductility, which should be absolutely avoided in the design of ductile joints; v) the influence of the shear action on the plastic behaviour of the material is disregarded; vi) prying forces are located at the edges of the T-stub flanges; vii) bending of the bolts is neglected; viii) cracking of the material is modelled by assuming the cracking condition as the occurrence of the ultimate strain in the extreme fibers of T-stub flanges.

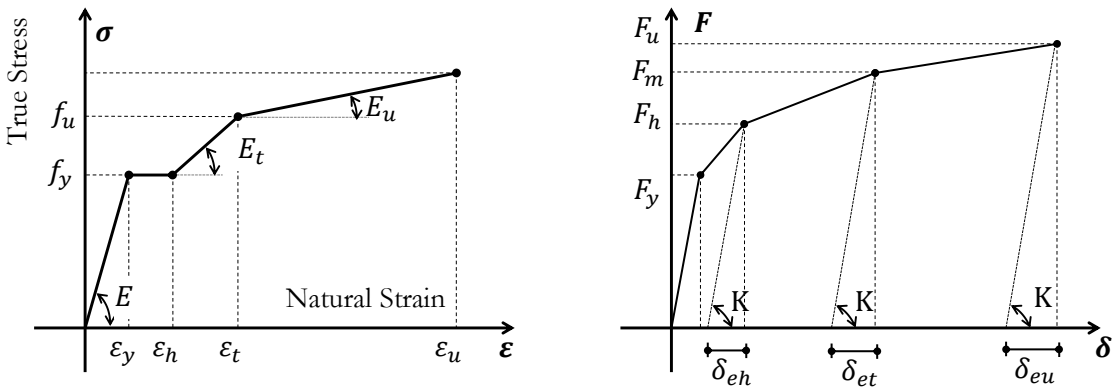

Figure 2.6 – a) Multi linear material description, and b) corresponding multi linear force versus displacement curve (Faella *et. al.,* 2000).

Most analytical procedures are developed based on the static equilibrium and application of the beam theory to the flange of the T-stub. Material non-linearity is usually taken into account based on bilinear description of material models and may include thermal softening and hysteretic behaviour if elevated temperature, (Simões da Silva *et al.*, 2002) (Spyrou, 2002), (Yu *et al.*, 2009), or cyclic loading cases (Pilluso & Rizzano, 2008) (Hu *et. al.*, 2012) are

studied, respectively. 3D effects are normally taken into account based on the effective width.

The analytical model developed by Yu and co-authors (Yu *et al.*, 2009) is further explored in Chapter 6 of this thesis as improvements to account for elevated strain rates are proposed.

2.3 Numerical studies

Finite element modelling of structural phenomena has been a common approach since the early 90's due to an incredible increase in computational capacity and due to the better understanding of how elements behave, thus allowing for mathematical representation. Gathering this information is a task that's been happening for decades and nowadays these mathematical approximations are either programmed by research groups or compiled into commercial software packages, allowing research groups to evaluate the behaviour of diverse phenomena by varying a model's properties with reduced cost.

Studying the behaviour of particular structural elements such as joints subjected to static loading, cyclic loading – for seismic evaluation – and subjected to fire hazard has been a target of research groups for the last couple decades using finite element models. The main objectives of these researches is to provide calibrated finite element models that can accurately reproduce experimental test results, vary the parameters within the model and develop additional guidance to actual design codes without having to perform a great amount of costly experimental tests.

Despite the advantages of modelling particular structural phenomenon and the information it provides to both designers and researchers, detailed finite element modelling is still an arduous task which requires a great amount of knowledge to verify the models representativeness of the real physics model.

Modern finite element simulations have had great development since Bursi and Jaspart (Bursi & Jaspart, 1998) published their article focusing on the simulation of extended end-plate joints. In their study the authors successfully reproduced the moment-rotation (M-Ø) relationship of bolted joints with extended end-plate subjected to monotonically increased displacement using the general purpose software, ABAQUS. Benchmark tests were conducted to establish constitutive relationships, step increment size, number of integration points, kinematic descriptions and study the effects of different finite element types and

discretization. The models included different constitutive laws for the flange, web, welds and bolt shank and simulations were conducted with elements C3D8, C3D8R, C3D8I. Finite element C3D8 is an eight-node brick element with full integration and 8 Gauss point which is accurate at the constitutive law integration level but may suffer from "*shear locking*" effects. These effects can be corrected with the use of elements with reduced integration (1 Gauss point), C3D8R, but then again, this type of elements is known for experiencing "*hourglass*" behaviour. Discretization with C3D8I (full integration and incompatible nodes) elements allows for 13 additional degrees of freedom and should be used in bending-dominated problems since it eliminates parasitic shear stresses observed in these problems. The results showed great accuracy using C3D8I elements, as the behaviour is governed by the T-stub created, which is a bending dominated problem, good approximation of the behaviour but underestimation of the results with the use of C3D8R elements, and inadequacy of C3D8 elements for this simulation

Several numerical studies on T-stub component under monotonic loading have been developed during the last years. In 2002, Swanson (Swanson & Leon, 2002) used ABAQUS software to perform a finite element analysis considering contact, and non-linear material and geometric characteristics. Good results in describing the experimental behaviour were obtained with a three-dimensional (3D) model; additionally, due to high computational cost of the 3D model, a 2D simplified model was developed to evaluate the effect of different pre-load levels in the bolts. The results showed that the initial stiffness is improved with increased pre-load force, but the ultimate failure load is not affected.

Experimental tests and numerical studies on welded T-stub component were conducted by Girão Coelho (Girão Coelho, 2004) (Girao Coelho, 2013). These studies were developed in order to evaluate the advantages of designing steel-frame buildings with partial strength and semi-rigid joints; several material and geometrical parameters were assessed. The experimental results showed that: (i) the deformation capacity primarily depends on the plate/bolt strength ratio and, (ii) the final collapse is governed by brittle fracture of the bolts, welds, or cracking of the flange near the weld toe. The FE models built using LUSAS provided accurate response of the T-stub behaviour up to fracture. The results showed that: (i) the magnitude of bolt and prying forces ratio to the applied load are increased for smaller weld throat thicknesses; (ii) changing the bolt gauge implies that the distance between yield lines also changes eventually shifting the governing plastic mode; (iii) as failure modes

progress from mode 1 to mode 3, resistance and initial stiffness increases, while deformation capacity diminishes; (iv) reducing the distance between potential yield lines produces stiffer behaviour; (v) increasing the flange steel grade would not improve joint stiffness (once elastic modulus remains unchanged) but it will naturally increase the T-stub resistance and eventually the post-limit stiffness; finally, (vi) it is noticed a decrease in the deformation capacity of steel flanges with higher grade, once bolt resistance eventually governs ultimate rupture.

2.4 Joint behaviour under impact loads

The previous sub-sections have highlighted the importance of providing an accurate description of how joints behave to fully assess the structural stability in avoiding progressive collapse. Particularly, studies concerning the T-stub model and the current analytical procedures used to define it's spring behaviour due to static loads have been discussed. Resistance and post-limit behaviour of joints due to accidental loadings are currently being investigated by the scientific community, yet most of the available studies are focused on fire (Santiago et al., 2008) and seismic hazard (Xu & Ellingwood, 2011). However, some research groups are recently focusing on the study of its behaviour under impact and blast loads. Efforts to account for joints' rotation capacity and post-limit strength when subject to accidental loading cases, particularly rapidly applied loads, are being undertaken by (Sabuwala & Krauthammer, 2005), (Yim & Krauthammer, 2009), (Daryan & Sadrnejad, 2011), (Urgessa & Arciszewski, 2011)(Stoddart, 2012) (Tyas *et al.*, 2012), (Stoddart & Tyas 2013).

Sabuwala and co-authors (Sabuwala & Krauthammer, 2005) performed 3D FE analyses to assess the behaviour of fully restrained steel joints subject to blast loads, performing validation against AISC program experimental results. The characterization of the blast load was made using SHOCK and FRANG codes. The elevated strain rate influence in steel's mechanical properties has been taken into account using dynamic increase factors as required by TM5-1300 (TM5-1300, 1991). Latter, in 2009, Yim and Krauthammer (Yim & Krauthammer, 2009) enhanced the study by conducting 3D FE analyses with solid elements on welded - unreinforced flange – bolted web (WUF-B) joints subject to several blast loads with duration ranging from 5 to 20 ms at different load levels. The authors propose that a load-impulse diagram, in which limit load and limit impulse are defined, to be established as

a joint's dynamic property. Simplified analyses of structural frame systems were made using connector elements (Abaqus, 2011) that accommodate the derived joint properties; the simplified frame models were able to maintain good accuracy for quasi-static and blast-rate loads, allowing alternative load path analysis of frames to be developed with low computational cost.

Similarly, Daryan and co-authors (Daryan & Sadrnejad, 2011) published a 3D dynamic FE study of seat angle bolted joint. Suggestions that TM5-1300 's verification criterion lacks a strength based criteria for steel joints subject to blast loads in addition to the one purely based on members rotation is made.

Urgessa (Urgessa & Arciszewski, 2011) developed a complex eight story steel frame model with S4R shell elements solved with ABAQUS/Explicit solver, loading the frame with an equivalent of 90.7 kg of TNT blast load and studied the behaviour of the frame with different joints setups, Figure 2.7. ABAQUS/Explicit enables the modelling of short, dynamic events with the advantage that it does not require the global tangent stiffness matrix to be calculated since it uses a lumped mass matrix approach which determines the acceleration of the node by its mass and net force, which reveals to be a more efficient method for an acceleration based problems rather than with ABAQUS/Implicit. The steel's constitutive law followed the Cowper-Symond overstress power to include the high-strain effect by applying a Dynamic Increase Factors (DIF) to the static stress-strain relationship.

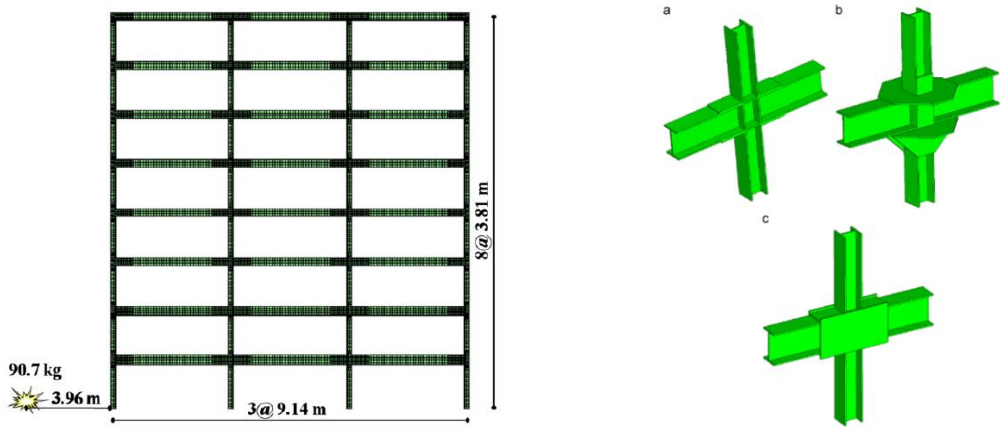

a) b)

Figure 2.7 – a) Steel frame modeled with S4R shell elements; b) different joint set-ups studied (Urgessa & Arciszewski, 2011)

In the event of a column loss the robustness of structures is achieved by catenary action of joints, and considering this accidental scenario, Yang (Yang & Tan, 2012) developed an

exhaustive study of six joint types, namely: i) web cleat; ii) fin plate; iii) top and seat with web angles (TSWA) 8mm, iv) Flush end plate joint; v) Extended end plate joint – Figure 2.8a); vi) TSWA 12 mm; performing numerical simulations with both *Implicit* and *Explicit* solvers included in ABAQUS. Based on previous experimental data, the authors were able to successfully develop a representative finite element model and then performed a parametric study to investigate the influence of joint depth on the rotation capacities, proposing four new joint acceptance criteria based on rotation capacity of the joints to withstand a middle column removal scenario – Figure 2.8b). The authors have also acknowledged that, although the increase of the joint depth would result in improvement of load-carrying and rotation capacity, the joint ductility may be adversely affected.

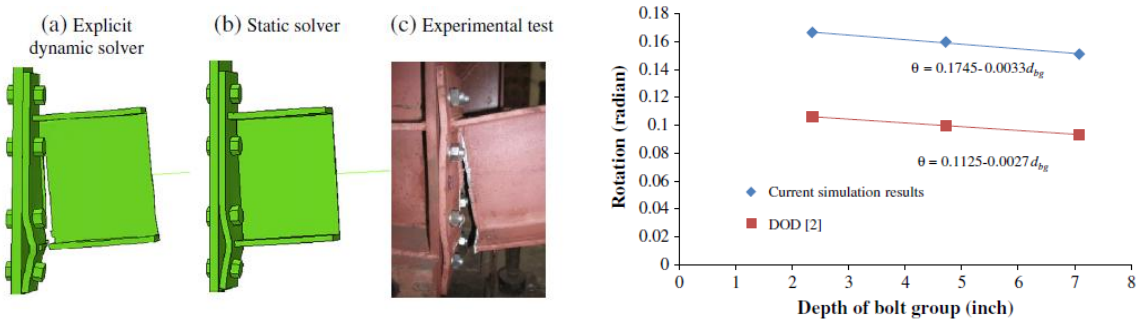

a) b)

Figure 2.8 – a) Comparison of FE simulations and experimental failure modes of extended end plate joint; b) Comparison of rotation capacity for web cleat joint: code criteria Vs. current simulations (Yang & Tan, 2012)

The computational models are very thorough and include fracture simulations. The finite element used is C3D8R type with mesh size of 5mm for bolts, angles or end plates, and 10 mm for beam and column elements. Special care was endorsed in material strain-stress relationships and in the convergence problems which generally appear in the *Implicit* solver when there are temporary instabilities of rigid body movement and numerous contact pairs are applied. A controlled artificial contact damping was employed but in fractured conditions the authors had to rely on the *Explicit* solver.

Recent efforts in this subject are being developed by a research group from the University of Sheffield where a joint testing set-up has been developed (Tyas et al., 2012) devoted to the study of the effects of impact loads. The testing facility has enabled the research group to address the resistance of fin plate joints subject to these kind of loads, and to develop component model in which the *bolt in shear* and the *fin plate in bearing* springs include the rate

dependant behaviour. The individual component springs are then combined in a spring model which is integrated in sub-frame models to perform non-linear dynamic analysis. According to the authors, this technique allows capturing the catenary action and the progressive fracture of the joint with reduced computational effort, and enhanced accuracy compared with the conventional method where axial and rotation springs are considered, (Stoddart, 2012), (Stoddart & Tyas 2013). Studies on flexible end plate joints subject to different levels of dynamic loading have also been conducted within the group (Chang & Tyas, 2011), taking the strain rate sensitivity into account. Fracture along the end plate close to the weld toe has been identified as the main failure mode for both static and dynamic loading, yet a relatively more brittle failure was observed when subject to dynamic loading.

3. MATERIAL CHARACTERIZATION

3.1 Static / hardening

Mild steel is macroscopically assumed as an isotropic material. Its constitutive characterization, for most engineering applications, can be obtained through quasi-static tension tests, from which the elastic modulus (E) and the elastic (f_y) and ultimate strengths (f_u) of steel are easily acquired.

Figure 3.1 presents the results from quasi-static uniaxial tension tests (Martins, 2012), conducted in accordance to the standard EN 10002-1 (EN10002-1, 2001) on a Universal Tensile Machine. During these tests, the load has been applied by controlling the induced displacement to reasonably low speeds (0.03 mm/s), to emulate the static response of the steel. Both mild steel coupon (solid blue line) grade S355 and quenched steel grade 8.8 (dotted red line) were conducted providing suitable material characterization for FEA described in this paper. The mild steel specimens have been collected from the same steel batch as the material used to prepare the tested T-stub specimens, while the steel grade 8.8 were picked from the same sales box of bolts M20. Three tests for each material were conducted; the mean results from the test campaign are presented in Table 3.1 and Figure 3.1. The solid blue curve denotes that mild steel is in nature a ductile material, with the capacity of absorbing great amount of energy before fracture; while the red dashed line which, despite its much higher elastic and ultimate strengths, exhibits rather low ductility capacity.

Concerning the stress-strain relationship for mild steel; it can be observed that the response exhibits firstly, a linear elastic development up to the yielding point where the elastic strength (f_y) is defined; afterwards the response is inelastic, meaning that the deformation is no longer recoverable, and the relationship becomes non-linear. This strain hardening phase is characterized by large deformations accompanied by the strength increase up to the

ultimate tensile strength (f_u). From this instability point on, the specimen will reduce its area due to the growth and coalescence of voids, visible through necking of the cross-section until fracture occurs; this phase of the stress-strain relationship is often referred to as the softening phase.

Table 3.1 – Material properties from uniaxial tension test

	E [GPa]	f_y [MPa]	f_u [MPa]	ε_y [%]	ε_u [%]
Steel S355	205.5	385	588	0.187	18.7
Bolt (8.8)	213.5	721.3	1002	0.337	2.3

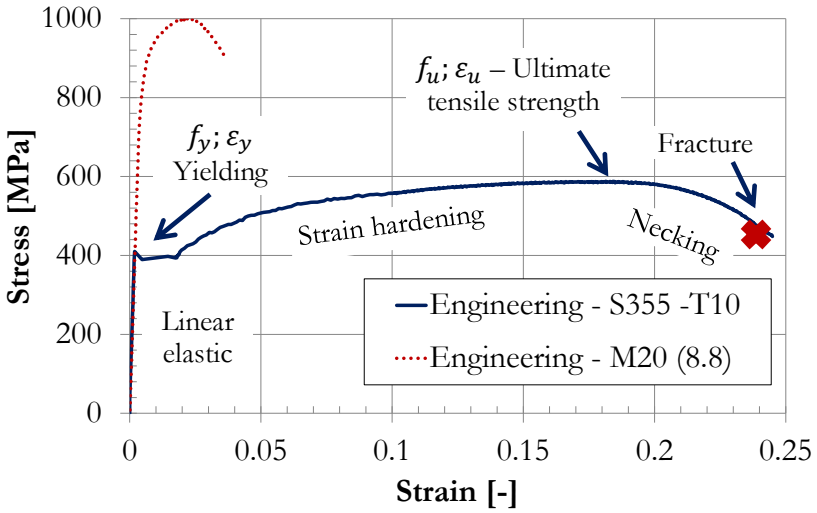

Figure 3.1 – Stress-strain relationship for S355 steel and bolt M20 (8.8)

3.2 Viscoplascity – Strain-rate

Strain rate is the deformation, *i.e.* strain variation, that a material is subject per time unit, $d\varepsilon/dt$. Most ductile materials have strength properties which are dependent on the loading speed; mild steel is known to have its flow stress affected (Dias da Silva, 2006). The effects of different strain rates on the stress-strain relationship of steel are illustrated in Figure 3.2. These true stress-logarithmic strain curves were obtained from an experimental programme carried out at the University of Coimbra, using a Compressive Split Hopkinson Pressure Bar (SHPB) for the dynamic tests (Saraiva, 2012) and the quasi-static tests. For the dynamic tests, an average strain rate around $\dot{\varepsilon} = 600$ s^{-1} was applied. Comparison against quasi-static results shows that:

i. the yield and ultimate strengths (f_y, f_u) increases near 50% the results

obtained under quasi-static loading;

ii. the total strain on rupture (ε_u) decreased, and;

iii. the elastic modulus (E) remains unchanged to the loading rate.

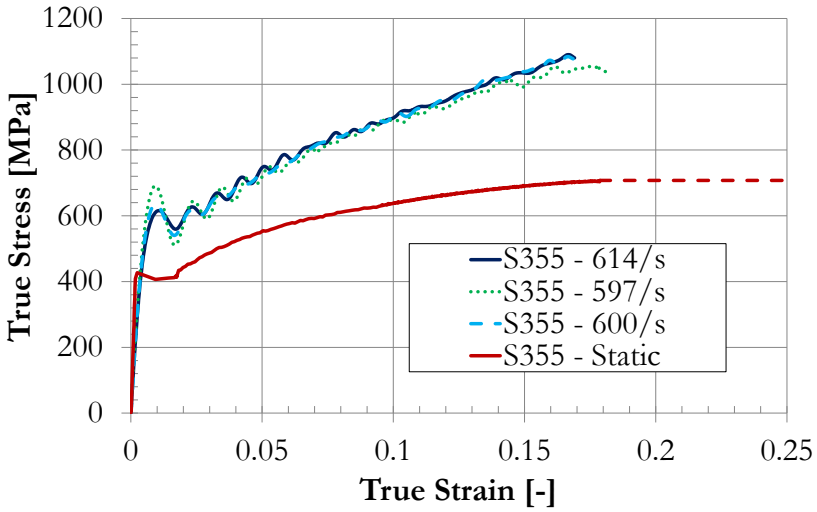

Figure 3.2 – True stress - logarithmic strain relationship of steel under high-strain rate (approx. 600 s^{-1}) for t = 15 mm plate, S355 (Saraiva, 2012).

A simplified way to consider high strain rate enhancement in the stress-strain material law is to adopt a dynamic increase factor (*DIF*), given by the relation of the dynamic strength, σ_{dyn} to the strength obtained under static conditions, σ_{static}

$$DIF = \frac{\sigma_{dyn}}{\sigma_{static}} \tag{6}$$

Finite element models aiming to simulate the behaviour of structural elements when subject to impact loads require a constitutive law representing the behaviour of materials for a range of strain rates. Amongst the most popular are the purely empirical Malvar model (Malvar & Crawford, 1998), Cowper-Symonds model (Cowper & Symonds, 1957) and Johnson–Cook model (Johnson & Cook, 1983) (see Appendix C). The latter accounts for the strain rate dependency and thermal softening behavior to establish the plastic behaviour. Its constitutive law assumes that the slope of flow stress σ, is independently affected by each of the mentioned variables (equation 2):

$$\sigma = [A + B\varepsilon^n] \cdot [\mathbf{1} + \boldsymbol{C\, ln\dot{\varepsilon}^*}] \cdot [1 - (T^*)^m] \tag{7}$$

where: A is the quasi-static yield strength; B and n represent the effects of strain hardening; m is the thermal softening fraction; $\boldsymbol{T^*}$ is a non-dimensional parameter defined based on the

melting and transition temperatures to take account for material softening due to temperature variation; ε is the equivalent plastic strain; $\dot{\varepsilon}$ is the strain rate; $\dot{\varepsilon}^* = \dot{\varepsilon}/\dot{\varepsilon}_0$ is the reference dimensionless plastic strain rate (assumed as $\dot{\varepsilon}_0 = 0.001\ s^{-1}$) and C is the strain rate constant.

Thus, based on the results from SHBT presented before and using the second term of Johnson–Cook's law (equation 2), C_{steel} = 0.039 for 600 s^{-1} is calculated to fit the experimental data (Saraiva, 2012) (Figure 3.2). The dependency on the strain rate of the bolts' material is accounted considering literature reports: impact tests on A 325 bolts recovered from the WTC debris exhibiting very low sensitivity to strain rate (Ellingwood, 2007), showing that high strength steels are less sensible to the effects of strain rate variation. According to Chang and his co-authors (Chang & Tyas, 2011), a dynamic increase factor DIF_{bolt} = 1.1 may be considered for the bolts. This value has been adopted in the current study, thus a value of C_{bolt} = 0.0072 is obtained. Nonetheless, the welds are assumed to have the same strain rate sensitivity as the base steel. Figure 3.4 provides the applied *DIF* for strain rate values between $0.001\ and\ 600\ s^{-1}$ following the Johnson–Cook law.

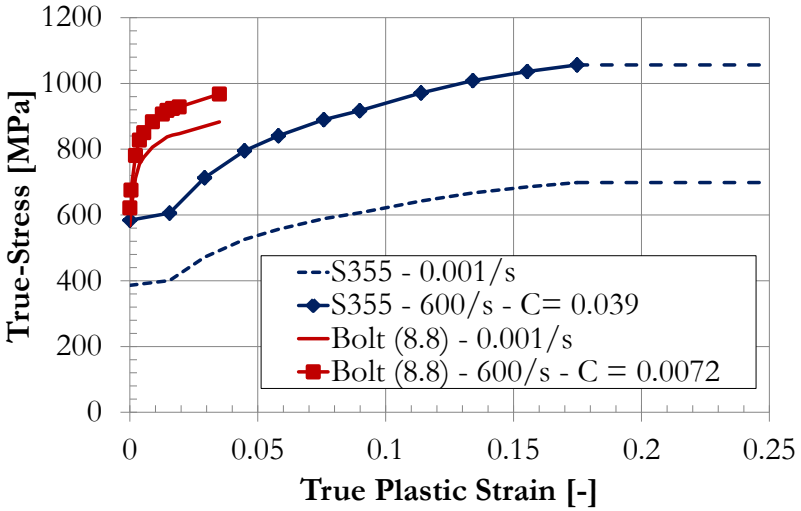

Figure 3.3 – Stress-strain relationship for mild steel and bolts considering strain rate sensitivity.

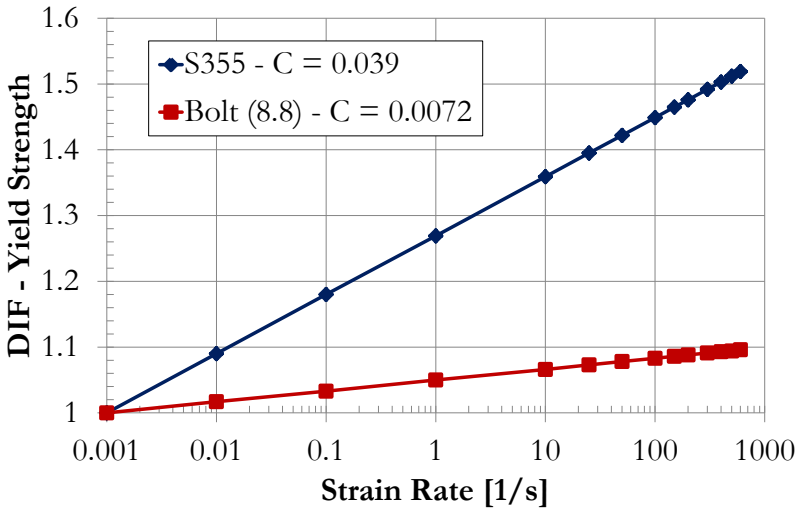

Figure 3.4 – Dynamic increase factor (*DIF*) of the yield strength as function of the strain rate.

3.3 Tenacity and toughness

Toughness is the ability of a material to absorb energy and plastically deform without fracturing; it is a property defined as the amount of energy per volume that a material can absorb before rupture. Thus, a material toughness can be understood as the area under the plastic region of the stress-strain diagram, Figure 3.5. High strength steels, shown in red colour, do not have clear a yielding zone where only plastic deformations occur, and, therefore, the onset of the plastic deformation is not evidently visible in the stress-strain diagram (Dias da Silva, 2006); the absence of plastic deformation eventually leads to a rather brittle behaviour.

The Eurocodes provide guidance concerning the selection of the material to avoid brittle behaviour as a function of the exploitation temperature. The characterization must be accomplished through *Charpy* and/or *Izod* impact tests on notched specimens measuring the fracture energy for a given temperature (EN 1993-1-10, 2005). This exploitation temperature is reduced as the strain rate imposed on the material increases, meaning that higher quality steels are required to avoid brittle failure when elevated strain rates are imposed.

The developed numerical model, however, does not take any variability of the material toughness into account although elevated strain rates are expected. The stress strain relationship is merely enhanced following the dynamic increase factors presented in the previous section, and the damage modelling (next section) is not fitted to account for variability of the material toughness to the strain rate.

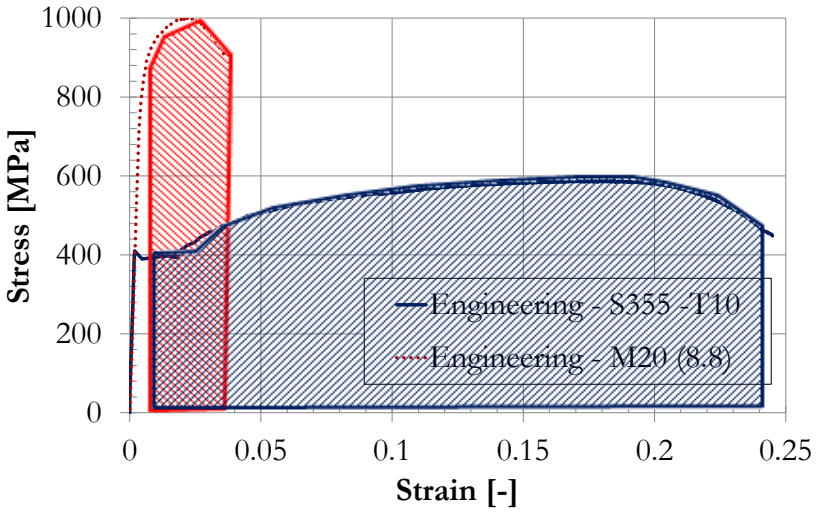

Figure 3.5 – Material toughness

3.4 Damage

Most metal alloys exhibit one of four types of fracture: fatigue fracture, cleavage fracture, intergranular fracture or ductile fracture. For materials with a stress-strain relationship represented by an elasto-plastic with isotropic hardening evolution, as for example the mild steel under quasi-static tension loading, failure is characterized by a ductile fracture mechanism (Lemaitre, 1992). The fracture is called ductile when it results from void nucleation followed by their growth and coalescence (Anderson, 1995).

Figure 3.6 presents the characteristic stress-strain behaviour of a material undergoing damage; the dashed curve represents a generic material response without damage definition, while the solid line corresponds to the damaged stress-strain relationship. In this figure, σ_y and $\bar{\varepsilon}_0^{pl}$ are the yield strength and equivalent plastic strain at the onset of damage, while $\bar{\varepsilon}_f^{pl}$ is the equivalent plastic strain at failure (Abaqus, 2011).

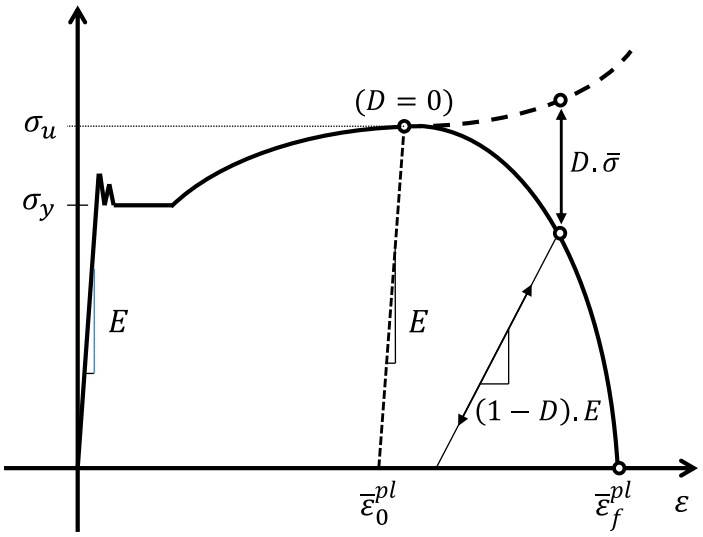

Figure 3.6 – Stress-strain curve with progressive damage degradation, adapted from (Abaqus, 2011).

Amongst other failure models to predict the beginning of damage, the formulation proposed by Hooputra and co-authors (Hooputra *et. al.*, 2004) is included in the software ABAQUS package (Abaqus, 2011), used to perform the reported FE analyses. The model assumes that two main relevant mechanisms can induce fracture of a ductile metal: i) *ductile fracture* due to nucleation, growth, and coalescence voids; ii) *shear fracture* due to shear band localization. In the presented models, only the model for ductile fracture is implemented; it assumes that the equivalent plastic strain at the beginning of damage, $\bar{\varepsilon}_0^{pl}$ is dependent on the strain rate and stress triaxiality, defined by $\left({}^{\sigma_H}/_{\sigma_{eq}}\right)$, where σ_H is the hydro static pressure stress and σ_{eq} is the equivalent Von Mises stress (see section §4.1.6). Additionally, a law establishing damage evolution is also required. Damage evolution description based on linear displacement requires the definition of the effective plastic displacement $\bar{u}^{pl} = L\,.\,\bar{\varepsilon}_f^{pl}$, where $\bar{\varepsilon}_f^{pl}$ is the equivalent plastic strain at failure and L is the characteristic length of the finite element; due to strain localization in elements situated in the necking development zone, the progressive damage response is mesh dependent (Abaqus, 2011). As elements reach a user defined level of degradation (for instance, the maximum degradation of $D = 1$) following $\sigma = (1 - D).\bar{\sigma}$, elements may be either kept or removed from the mesh. Hooputra and co-authors (Hooputra *et. al.*, 2004) advise that the procedure is suitable to predict crack initiation zones, but that element removal should be regarded as preliminary assessment for crack propagation simulation.

3.4.1 Failure modelling

Implementation of the failure criterion discussed above is assessed on a simple uniaxial quasi-static tensile test with t = 10 mm thickness. The experimental strain-stress material properties are obtained from the mechanical extensometer with an initial gauge length L_0 = 30 mm (Figure 3.7 d)). Measurement of the final gauge length after fracture is L_u = 42 mm, corresponding to a total extension after fracture equal to 40%.

The geometry and FE mesh of the numerical model follows the dimensions of the tested coupon (width x thickness = 20 x 10 mm^2). The model is built with three-dimensional 8-node linear brick solid elements C3D8R, and a static general analysis with displacement based loading is used. Symmetry conditions are taken into account, therefore only a quarter of the coupon is modelled. Typically a structured mesh technique is employed; the meshing constraints lead to an element size of 1.5×1.5×1.2 mm^3 at mid height of the specimen (Figure 3.7 a) and b)). This numerical model is able to describe the material behaviour and to predict the failure experimentally observed (Figure 3.7 c) and d)). Figure 3.7 c) shows an increment within the softening phase with the damage scalar variable pattern (SDEG): elements with $D \geq 1.0$ have been deleted, while the deformed mesh clearly exhibits necking in the gauge length.

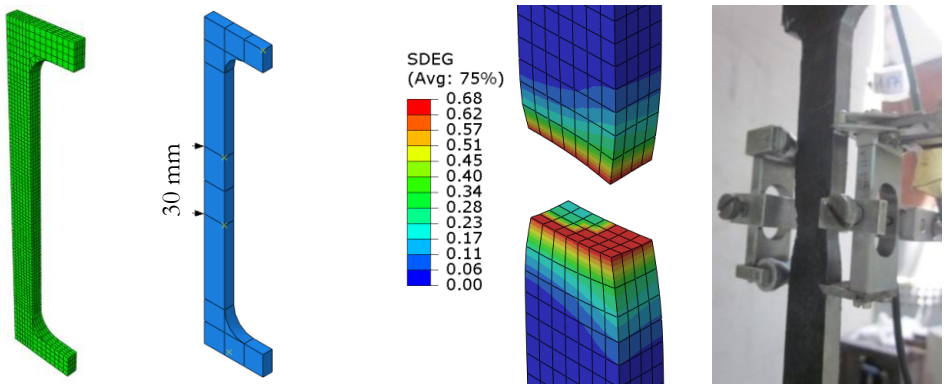

a) b) c) d)

Figure 3.7 – a) Finite element model representing 1/4 of the coupon test; b) gauge length; c) scalar damage pattern; d) uniaxial coupon test.

Figure 3.8 represents the procedure developed for modelling the material:

i. blue curve - the material curve obtained through the uniaxial quasi-static tensile test: *Engineering - S355 - T10;*
ii. green curve - strain-stress relationships obtained from the numerical model without progressive damage definition: *Numeric – No Damage*;

iii. red curve - strain-stress relationships obtained from the numerical model considering a strain at rupture of 18.7% (in accordance with Table 3.1). The damage evolution, as defined previously, has been set to follow a linear law with an effective plastic displacement of $\bar{u}^{pl} = 1.5$ mm. The numerical curve matches the experimental one very closely: *Numeric – (l_0=30) – u = 1.5*.

This model allows the calibration of the equivalent plastic strain at the onset of damage, $\bar{\varepsilon}_0^{pl}$ for the stress triaxiality ratio for pure tension of $\sigma_H/\sigma_{eq} = 1/3$. The equivalent plastic strain for other triaxial stress states have been extrapolated, following the formulation included in the ductile damage failure model by Lemaitre (Lemaitre, 1992).

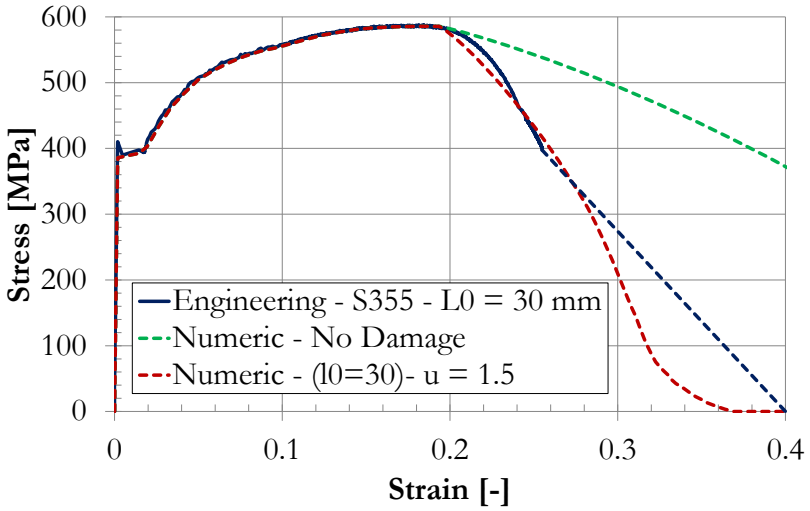

Figure 3.8 – Damage model assessment: Comparison of the stress-strain relationship obtained by experimental tests and numerical simulations.

4. FINITE ELEMENT MODEL

4.1 FINITE ELEMENT METHOD

4.1.1 Introduction

The finite element method is a numerical tool used for the approximation of multiphysics problems. With the current increase in computational capacity, finite element analysis have become a primary tool in the solution of complex engineering problems; given a system and its boundary conditions, its behaviour can be approximated through the solution of the algebraic equations governing its behaviour (Bathe, 1996), (Hutton, 2004). For a static calculation the main equation may be reduced to eq. (8).

$$K.u = F \tag{8}$$

where K is the stiffness matrix, u the vector of unknown displacements and F the external force vector.

One fundamental step in the finite element method is the discretization of the system's domain into a number of finite-size domains; usually a higher number of small finite-size domains yield better approximation of the solution, however at the cost of higher computational effort.

Current common applications of the finite element method range from structural analysis, heat transfer and fluid flow; nevertheless its basic principle ought to be applicable to any discretizable system, which behaviour can be approximated through a mathematical function.

The state of the art about the finite element method is vast and generally out of the scope of current thesis. However, this chapter provides insight to the particular tools used to establish the finite element model described later. The finite element model describes a geometric and

material non-linear response of the T-stub model and, given the objective of modelling the response to an impact load, the dynamic transient response is required.

Generally the non-linear response of a system may be solved through the implementation of an incremental procedure Figure 4.1. While for static conditions the Newton-Raphson (or any modification of the method) can meet convergence criteria and establish the response of the studied system, for transient dynamic situations it is no longer of use. Transient dynamic solvers are divided in two main categories: *implicit* and *explicit*; both types of procedures are implemented in the ABAQUS (Abaqus, 2011) code and the differences and advantages between in using both are explored in this chapter.

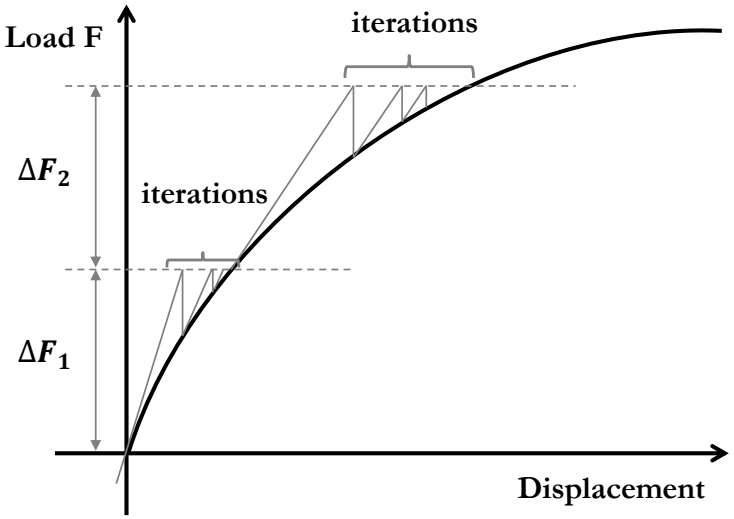

Figure 4.1 - Incremental non-linear procedure

4.1.2 Non-linear dynamic Analysis

Non-linear dynamic analyses are required to be performed in a time domain. In turn, this means that the inertial effects of a mass cannot be disregarded (in opposition to static conditions) and therefore the dynamic properties, acceleration and velocity, must be accounted for. The transient behaviour description of a mass follows the Newton's 2nd law of motion $F = M.\ddot{u}$. In non-linear dynamic analysis field this equation is mostly known in the form of eq. (9)

$$M.\ddot{u} + C.\dot{u} + K.u = F \tag{9}$$

where M is the mass matrix for each element, C the viscous damping and K the stiffness matrix, while $u, \dot{u}, \ddot{u}$ are the displacement and its first and second derivatives, velocity and acceleration, respectively, for each each element.

Two different solution strategies are available to perform non-linear dynamic analysis: *implicit* and *explicit*. Implicit procedures are related to solution schemes that require the solution of a system of equations for evaluation of u_{n+1}; whereas explicit procedures are those in which evaluation of u_{n+1} can be directly obtained from the previous steps and do not require the solution of a system of equations; *i.e.* equation (9) is integrated in very small time increments.

The Hilber-Hughes-Taylor (HHT) is a well-established implicit numerical procedure for the direct integration of the equations of structural dynamics. The HHT method provides dissipation combining the positive Newmark ϒ-dissipation and negative α-dissipation methods, with improved characteristics ensuring dissipation of the higher frequencies while the lower modes are not affected too strongly. Moreover, the HHT algorithm is unconditionally stable with respect to Δ_t/τ (time-increment/period) whenever $-0.5 \leq \alpha \leq 0$, thus allowing for relatively large time-increments (Hilber *et. al.,* 1977).

Explicit procedures using central-differences integration rule, are conditionally stable with respect to the time-increment; usually, very small time increments are necessary. However, each increment is relatively inexpensive as the central-differences integration rule uses a lumped mass matrix avoiding the assembly and solution of a set of equations; furthermore, this simplification allows the reduction of spurious oscillations as opposed to the use of a consistent mass matrix (Abaqus, 2011).

Considering an hysteretic analysis of bolted beam-to-column joints, differences in the use of both integration schemes have been addressed by Vegte (Vegte & Makino, 2004) in terms of: i) solution strategy; ii) computational time with respect to the model size Figure 4.2, and; iii) convergence in non-linear contact. Vegte recommends the explicit procedure for solving large models with reduced computational cost and for handling non-linear contact with ease: simulations run with very general contact definitions, once equilibrium and contact constrains checks do not need to be met.

4.1.3 Implicit vs. Explicit

ABAQUS\standard has been used in this work to run dynamic analyses; it performs direct integration using the mentioned Hilber-Hughes-Taylor (HHT) integration procedure (Hilber *et. al.,* 1977). A moderate dissipation application is chosen for its purpose related to impact analysis, allowing for moderate amounts of energy to be dissipated by plasticity or viscous damping; the moderate dissipation application sets HHT parameters to $\alpha = -0.41421$;

$\beta = 0.5$ and $\gamma = 0.91421$ (Abaqus, 2011), thus within the range to be unconditionally stable with respect to the time-increment.

ABAQUS\explicit is has been explored looking forward to optimise the computational runtime for future numerical simulations of larger models of full joints. When compared to an implicit procedure, an explicit algorithm is advantageous for (Vegte & Makino, 2004), (Abaqus, 2011):

i. allowing very general contact properties;
ii. not requiring convergence criteria and contact constraints to be met;
iii. not performing iterations nor forming tangent stiffness matrices;
iv. not requiring the solution of a set of equations.
v. rising the computational cost linearly to the number of degrees of freedom, Figure 4.2.

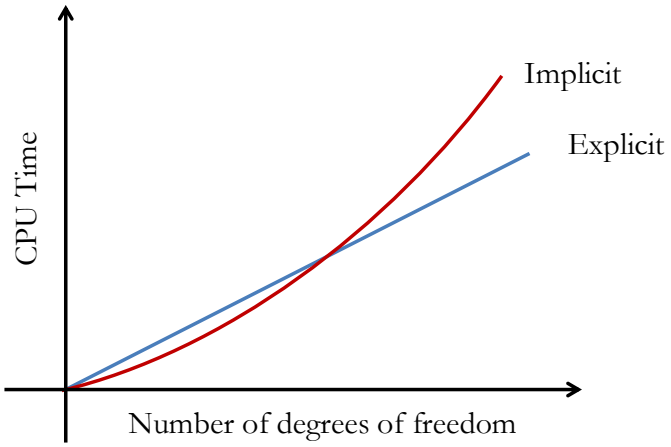

Figure 4.2 – Implicit Vs. Explicit computation time scheme (Abaqus, 2011)

These advantages allow i) to smoothly advance within the analysis of highly non-linear systems, and ii) set the explicit procedure as best suited for large models, especially when studying very short time events. A major drawback of the explicit dynamics procedure is that the results are not automatically checked for accuracy; therefore it is up to the user to verify the energy balance to validate the response (Abaqus, 2011).

Previous trial runs of an explicit analysis of T-15, the stable time increment has been found to be of 1.79E-08 s, conditioned by elements situated in the web; such small stable time increment requires 55866 time increments for 0.001 s of the analysis runtime (1/20 of the complete 20 ms analysis). With the implicit dynamic procedure the time increment demonstrated to be much higher whilst yielding reliable results in shorter wall clock runtime;

taking into account that this is a rather small model, the implicit procedure would be the preferred choice to obtain the response.

4.1.4 Finite element typology

The finite element models presented later are generally built with solid brick elements. "Reduced" numerical integration, first order elements are generally considered, C3D8R – Figure 4.3. Containing only one Gauss integration point, their reduced integration scheme follows the "*uniform strain formulation*": *i.e.* the strains are not obtained at the first-order Gauss point but are obtained as the analytically calculated average strain over the element's volume (Abaqus, 2011). Following this formulation, first order reduced integration elements yield the exact average strain over the element volume simplifying the interaction with the non-linear constitutive routines. C3D8R elements contain 8 nodes and 3 degrees of freedom per node.

Each finite element type has its numerical integration difficulties (Bursi & Jaspart, 1998), (Sun, 2006). When subject to bending fully integrated first order brick elements may suffer from "shear locking" problems and reduced integration elements are prone to suffer from "hourglassing" behaviour. A short explanation of these behaviours is provided:

Shear locking: as an element is subject to bending, it should deliver a shape keeping the rectangular angle; however fully integrated first order brick elements are unable to bend its edges delivering a shape unable to maintain the angle rectangular, see Figure 4.4 a); this causes the appearance of incorrect artificial shear stress and shear deformation instead of bending deformation, therefore fully integrated first order brick elements should not be used whenever bending behaviour is required.

Hour glass: hourglass behaviour may be exhibited by reduced integration element when subject to bending; despite their nodal deformation remains similar to fully integrated first order brick elements, the lines passing in its integration point will remain unchanged Figure 4.4b). In turn this means that normal and shear stresses are zero and that there is no strain energy generated by the deformation. Abaqus uses the artificial stiffness method and the artificial damping method control the hourglass modes in these elements (Abaqus, 2011).

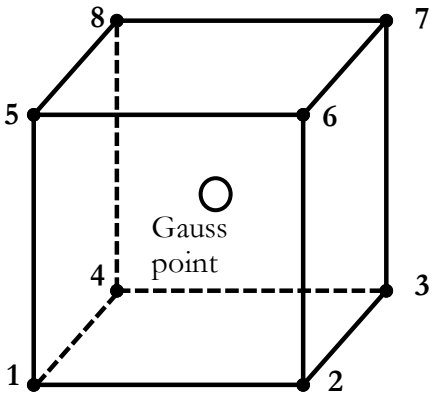

Figure 4.3 – Reduced integration 8-node brick element

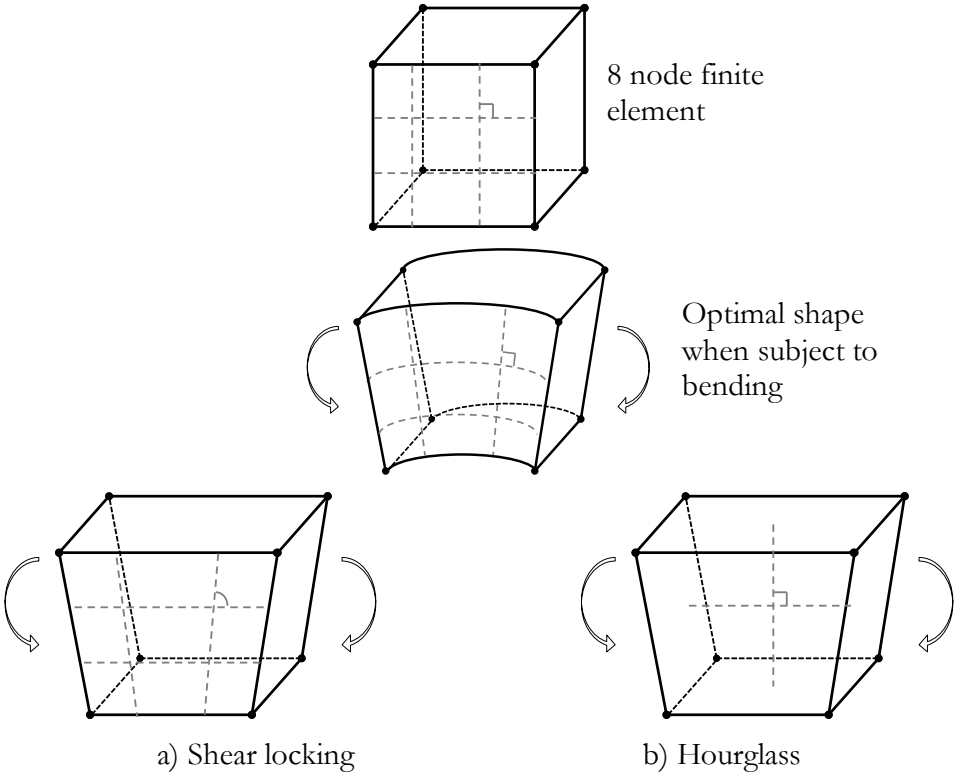

Figure 4.4 - Numerical integration problems of elements subject to bending:
a) shear locking; b) Hourglass. (Sun, 2006)

4.1.5 Contact algorithm

Modelling of steel joints requires the simulation of the contact between the multiple connecting elements; the most common concern the interaction between the bolts and the hole surfaces, and the end-plate surfaces. The interface contact modelling can be accomplished with ABAQUS (Abaqus, 2011) with finite-slide interaction between deformable bodies by providing a master-slave relation between interacting surfaces; for the case in hand normal and tangential contact properties ought to be provided.

Normal contact properties are accomplished with "*hard-contact*" property allowing for separation after contact; the tangential behaviour has been assumed with a friction coefficient of *0.2* following "*penalty*" formulation for the Coulomb frictional behaviour definition. In this way, the critical shear stress due to tangential contact between surfaces before slip is allowed, while it is dependent on the contact pressure. The slip, itself, is considered to be linear and isotropic (Abaqus, 2011).

4.1.6 Von Mises yield criterion

Material hardening is introduced in the numerical model by means of multilinear description of the strain-stress curves measured experimentally. The transition from elastic to plastic phases is computed following the isotropic material model included in the software. The Von Mises yield criteria used (Abaqus, 2011) to establish the yield surfaces states that a ductile solid will yield when it's the distortion energy reaches the material critical value, as illustrated in Figure 4.5 and eq. (10). Following this criteria, the yield condition is independent of the hydrostatic stresses as long as the triaxial stress state is kept to a low level (absence of voids).

$$\sigma_{Von\ Mises} = \sqrt{\frac{\left(\sigma_{xx} - \sigma_{yy}\right)^2 + \left(\sigma_{yy} - \sigma_{zz}\right)^2 + (\sigma_{zz} - \sigma_{xx})^2 + 6\left(\tau_{xy}{}^2 + \tau_{yz}{}^2 + \tau_{zx}{}^2\right)}{2}} \quad (10)$$

In parallel, the equivalent plastic strain, $\bar{\varepsilon}^{pl}$, provides the amount of permanent strain installed in a finite element, eq. (11).

$$\bar{\varepsilon}^{pl} = \frac{1}{1+\nu'}\sqrt{\frac{(\varepsilon_1 - \varepsilon_2)^2 + (\varepsilon_2 - \varepsilon_3)^2 + (\varepsilon_3 - \varepsilon_1)^2}{2}} \quad (11)$$

Where ν' is the effective Poisson's ratio, computed as material's Poisson's ratio ($\nu' = 0.3$ for elastic strains and $\nu' = 0.5$ for plastic strains, in the case of steel).

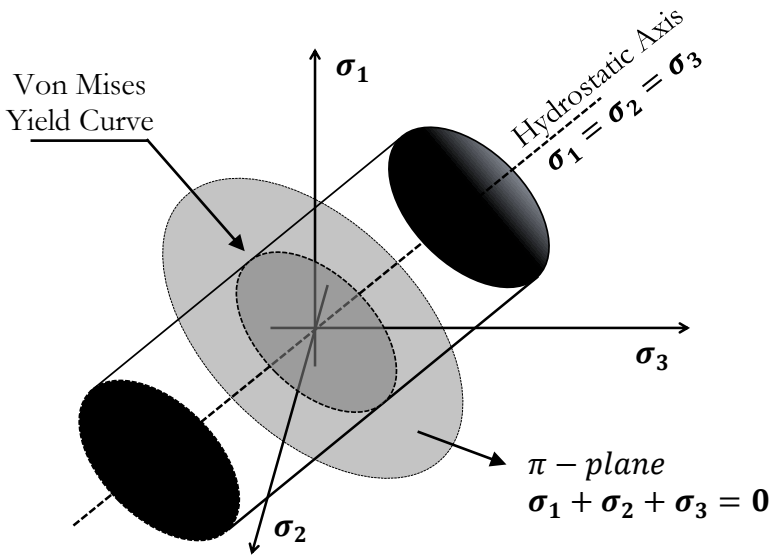

Figure 4.5 – Von Mises yield criteria

4.2 Description of the structural model

The T-stub model analysed consideres the study being carried out at the University of Coimbra under research project "ImpactFIRE". The test set-up used in the experiments is depicted in Figure 4.6 and further description can be found in (Barata *et al.*, 2014a). It consists of a very stiff structure (shown in grey colour) anchored to the floor. The loading mechanism is based on the principle of a 2nd class lever. The yellow beam is loaded in one end (point C) by a loading device (red colour) and it rotates around the pivot axis in the other end (point A). The tested T-stub (shown in blue in the middle of the testing layout, point B) (Figure 4.7) is limited by two additional pins at its end, assuring the transfer of axial tensile forces only. Figure 4.7 shows a T-15 specimen equipped with the deflectometer (for deformation measuring) ready for a quasi-static testing; the measuring point is on top surface of the T-stub's flange.

During the quasi-static tests, the loading device is a servo actuator with 1000 kN capacity, whilst during the dynamic tests, a tank is filled with gas, up to a pressure of 30 MPa (300 Bar). Once the pressurized gas is released into the chamber, shown in red, the gas accelerates a ram with approximately 40 kg of mass that impacts the yellow beam.

The dynamic equilibrium of the system is established measuring the beam's acceleration and displacements, and the transient applied load. The instrumentation includes an accelerometer placed in the mass centre of the beam (point B), and another accelerometer, a

load cell and a laser distance gauge located in the load application point (point C). Two additional laser distance gauges are used to measure the T-stub's opening.

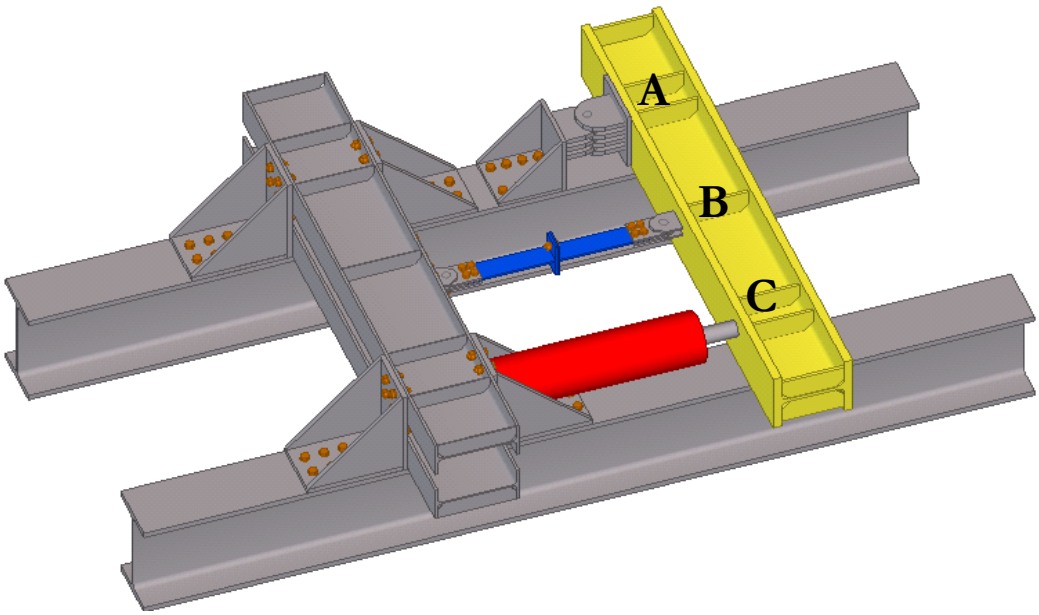

Figure 4.6 – Experimental test layout (Barata *et al.*, 2014a)

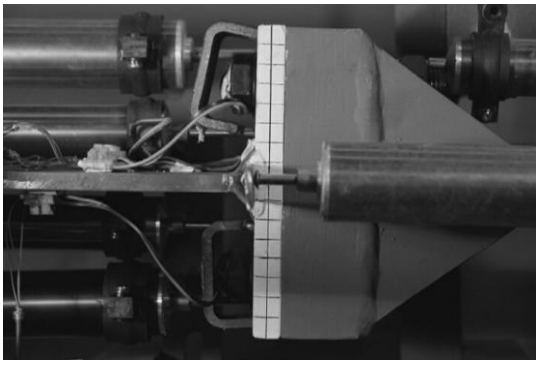

Figure 4.7 – T-stub specimen previous to quasi-static test.

4.3 Description of FE model

The T-stub model analysed in this paper is a simplified, individualized and symmetric geometry of the T-stubs developed in a current beam-to-column joint; Figure 4.8a) illustrates an example of a T-stub extracted from a beam-to-column joint. The tested T-stub dimensions are presented in Figure 4.8b); two T-stubs are studied: flange thickness equal to 10 and 15 mm; the steel grade is S355 and the bolts M20 grade 8.8 are fully threaded. Figure 4.9 shows the numerical model's boundary condition and mesh discretization.

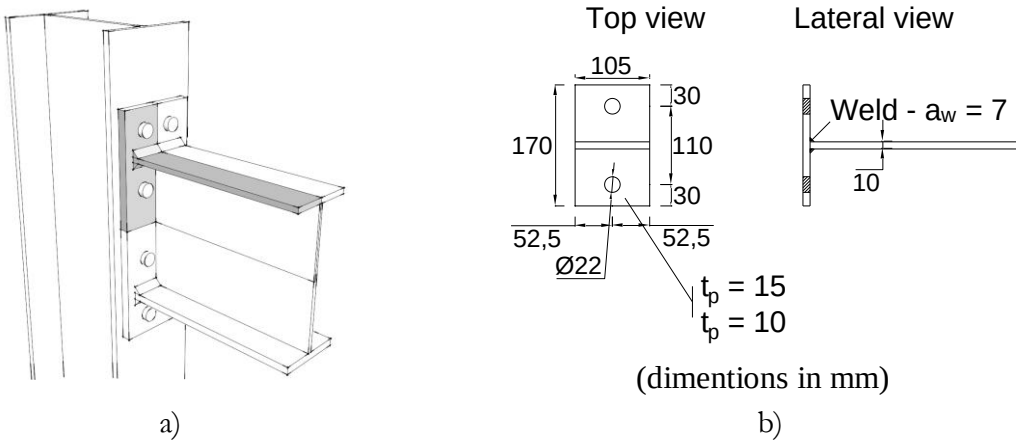

Figure 4.8 – a) T-stub fragment from a beam-to-column joint; b) T-stub geometry;

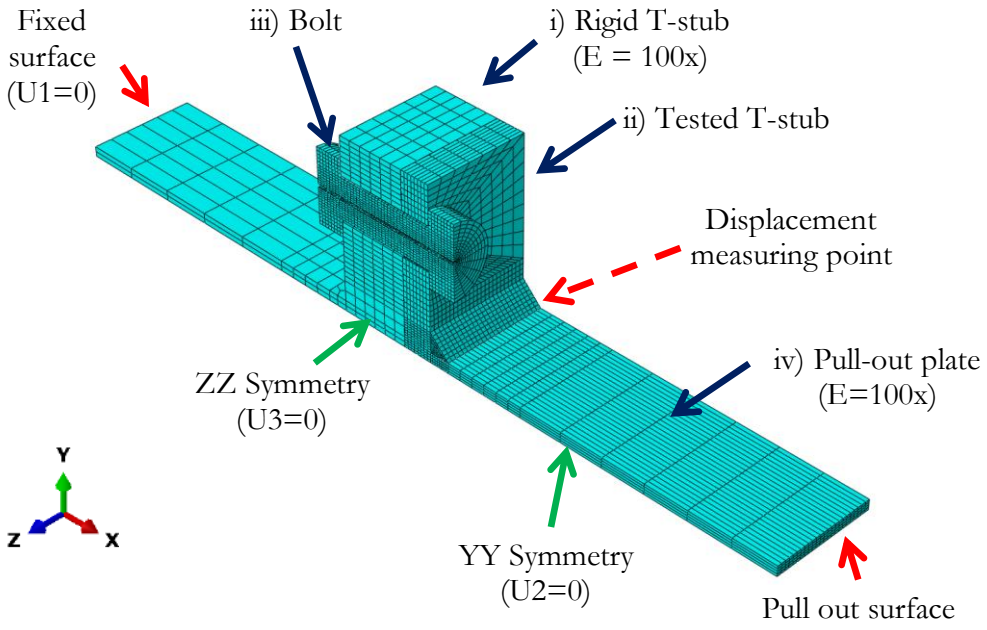

Figure 4.9 – Numerical model, boundary condition and mesh discretization.

The FE analyses are conducted with the software ABAQUS (Abaqus, 2011). The FE model is composed of four parts: (i) rigid back T-stub; (ii) tested T-stub; (iii) bolt, (head and shank as a single piece) and (iv) pull-out plate (web), as depicted in Figure 4.9. Contact conditions are accomplished through a master-slave relationship, modelled between all the four parts namely: (i) the bottom flange surface with the back T-stub bottom flange; (ii) bolt shank with flanges bolt hole; (iii) top flange surfaces with bolt head; and (iv) pull out plate contact with the tested T-stub flange once the welds showed very little penetration (thus the plates are not necessarily in contact). The welds are modelled in the tested T-stub part and connected to the pull out plate with a tie constraint property. As stated in the previous

chapter, normal contact conditions are accomplished with "hard-contact" property allowing for separation after contact and the tangential behaviour is assumed with a friction coefficient of 0.2 following "penalty" formulation for the Coulomb frictional behaviour definition. Bolt modelling follows the nominal geometry (bolt shank diameter of 20 mm and the hole diameter 22 mm) and no pre-load is considered.

The T-stub model has been simplified by the use of symmetry conditions in axes *yy* and *zz*; therefore, displacements in these directions are restrained at the symmetry surfaces (Figure 4.9). The model is generated with solid element type C3D8R (first order reduced integration continuum element), allowing for non-linear geometrical and material behaviour. C3D8R is a valuable choice due to its reduced integration (only 1 integration point) allowing for reductions in calculation time, while it provides hour-glass behaviour control. Generally a structured mesh technique with "Hex" element shape is used, except for the weld zone where a "Wedge" element shape is employed.

Mesh sensitivity analyses were previously conducted assuring that a discretization of at least 4 elements through the thickness of bending-dominated plates (T-stub flanges), and a concentrical mesh around the bolt area of at least 8×6 (edge × diagonal) elements provided accurate results, whilst reducing computation time and convergence problems. On the other hand, in zones where the strain gradients are negligible (near the end of the webs), a coarser mesh has been used.

4.4 Pulse loads and dynamic properties

Commonly, structural verification is accomplished through the static representation of loads, meaning that the load application time (or the *force magnitude vs. time* function) is disregarded. The effects of static loads are easily calculated once the imposed acceleration and induced vibrations are disregarded. However when the load application time is reduced to very small time increments, the imposed accelerations (and velocities) must be taken into consideration thought the application of the *impulse-momentum* principle (Szuladziński, 2010).

The effects of short transient loads are, therefore, dependent on the natural vibration frequency of the affected system. When a load is applied in a time shorter than 10% of the system's natural period, ($t_0 < 0.1\tau$), are referred to as impulsive loads (Szuladziński, 2010). According to (Cormie & Smith, 2009) three regimes can be distinguished:

Impulsive: $t_0 < 0.1\tau$

Dynamic: $0.1.\tau < t_0 < 10.\tau$

Quasi-Static: $10.\tau < t_0$

Where t_0 is the pulse duration and τ the natural period of the system.

Commonly four basic types of blast and impact pulse load schemes are considered t, Figure 4.10. The rectangular pulse (Figure 4.10a) describes two possible situations: "*instantaneous*" loading in solid line, and "*sudden*" loading in dashed line.

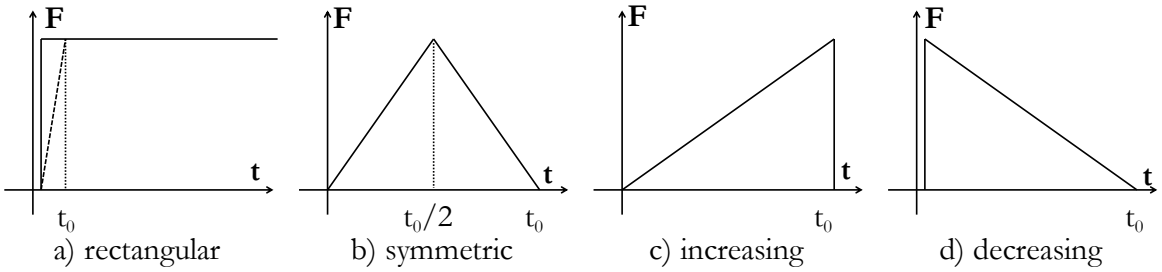

Figure 4.10 – Blast and impact pulse load schemes (Cormie & Smith, 2009), (Szuladziński, 2010)

Considering the dynamic properties of the developed models, Figure 4.11 and Figure 4.12 present the displacement contour (*U*) for the first natural frequency of the for T-stub flange thickness of 10 and 15 mm, (T-10 and T-15, deformation is scaled 20x). The linear perturbation problem is solved using the *Subspace* solver to extract the eigenvalue of the system (Abaqus, 2011). The first frequency ($f = 1/\tau$) for model T-10 is 1375 /s ($\tau_{T-10} = 7.3\,E^{-4}\,s$), and for T-15 is 1734 /s ($\tau_{T-15} = 5.8\,E^{-4}\,s$. This means that impulsive responses are achieved for load application times, t_0, around 0.06 ms.

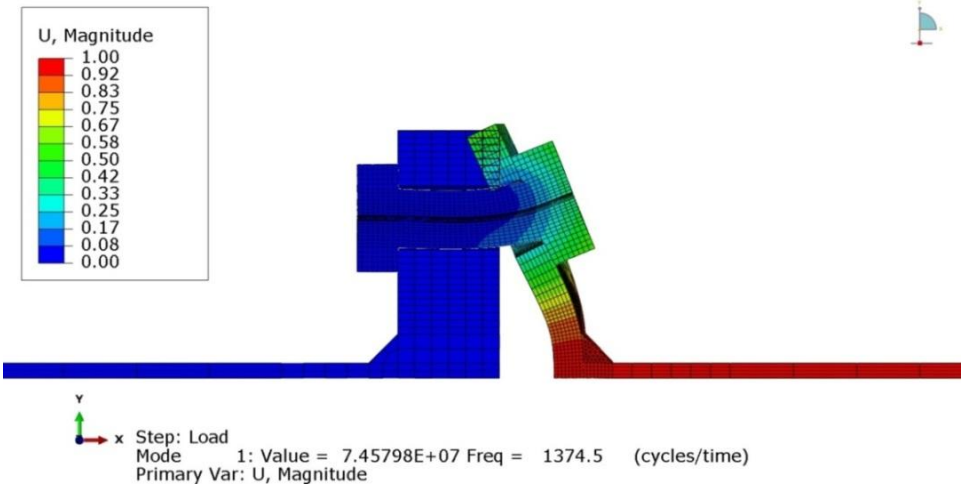

Figure 4.11 – T-10 model. 1st frequency mode (scaled 20x): 1375 cycles/s

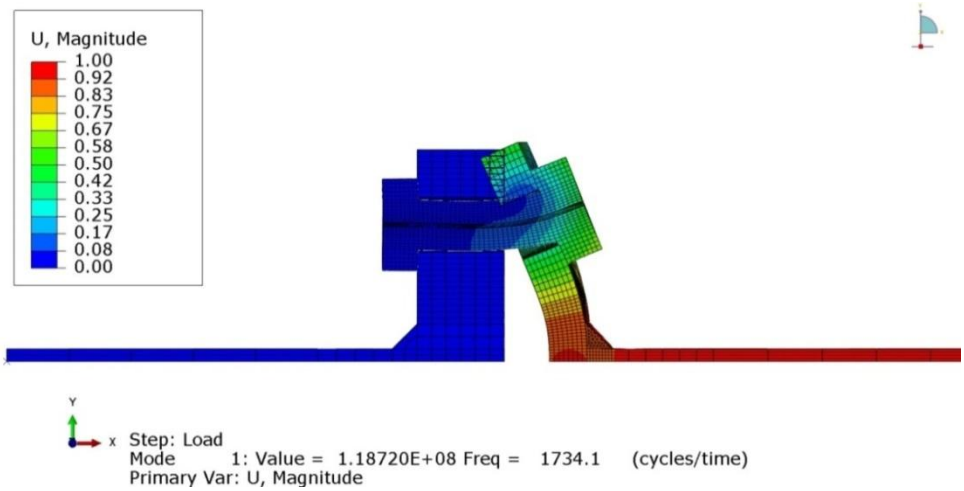

Figure 4.12 – T-15 model. 1st frequency mode (scaled 20x): 1734 cycles/s

4.5 Material Properties

Material nonlinearity is included by specifying a non-linear stress-strain relationship for material hardening; Von Mises criterion is considered to establish the yield surfaces with the associated plastic flow for isotropic materials (Abaqus, 2011). In order to consider large strains and large displacements, the monotonic stress-strain relationships obtained in the previously mentioned uniaxial coupon tests for the steel and for the M20 grade 8.8 bolt (Chapter §3), have been employed in the *true-stress – logarithmic plastic strain* form – Eqs. (12), (13) and Figure 3.4.

$$\varepsilon_{true} = ln(1 + \varepsilon_{eng}) \tag{12}$$

$$\sigma_{true} = \sigma_{eng}\ (1 + \varepsilon_{eng}) \tag{13}$$

Once the bolt geometry follows nominal dimensions, bolt material properties have been updated to take into account the reduced tensile shank area. Material properties for the weld are assumed equal to the base steel plates. For the study of the effects of impulsive loads, DIFs reported previously (section §3.2) are employed.

Material behaviour includes the ductile failure modelling presented previously for both the steel and the bolt. For the latter, the equivalent plastic strain dependency to the triaxiality stress state is built considering a strain at rupture of 30%. For the linear damage evolution description, a reduced effective plastic displacement of $\bar{u}^{pl} = 0.1$ mm is used due to the bolts' rather brittle behaviour. Despite the possible differentiate behaviour, damage properties remain the same when studying the behaviour of T-stubs subject to impulsive

loads. Figure 4.13 presents the dependency of the equivalent plastic strain (PEEQ) to the triaxial stress state used to define the onset of damage for both materials.

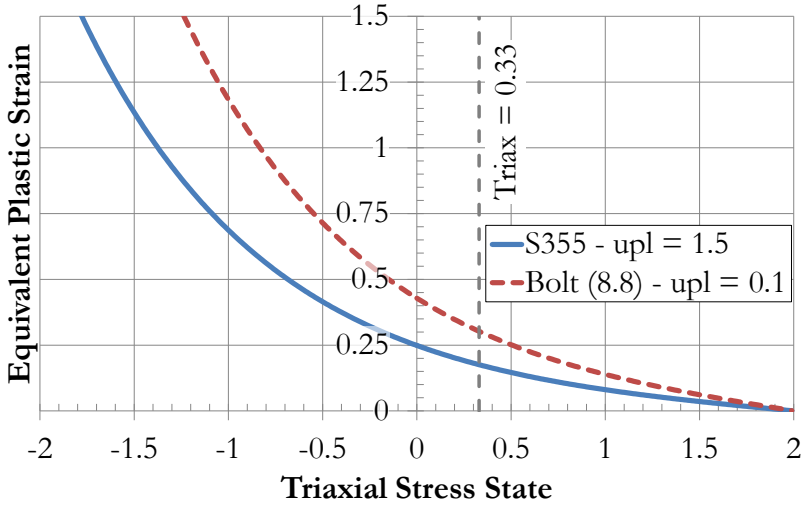

Figure 4.13 – Equivalent plastic strain – triaxial stress state dependency for the onset of damage.

PART II

T-STUB BEHAVIOUR UNDER IMPACT LOADING – Numerical Approach

T-STUB BEHAVIOUR UNDER IMPACT LOADING – Analytical Approach

CONCLUSION

5. T-STUB BEHAVIOUR UNDER IMPACT LOADING – NUMERICAL APPROACH

5.1 Validation under monotonic loading

The validation of the numerical model establishing the non-linear response of T-stubs (T-10 and T-15) is based on the experimental results from Barata and co-authors (Barata *et al.*, 2013). Under static loading, the experimental response was reached using two similar test specimens for each T-stub, Test#1 and Test#2. The load was gradually applied under displacement control with a speed of 0.02mm/s up to failure of the specimen. The "displacement control" is used in FEA up to fracture.

Figure 5.1 compares the numerical (T-xx-DynQS) with the experimental response (T-xx-Test#1 and Txx-Test#2). It can be observed that the numerical models accurately predict the global behaviour of the T-stub component: the elastic stiffness and the plastic transition are well defined. Table 5.1 compares the design values obtained from analytical calculation according to Eurocode 3, Part 1.8 with experimental results and numerical predictions. Estimation of the design resistance (experimental and numerical) is calculated using a bilinear approximation of the force-displacement curve based on the initial and post-limit stiffnesses ($K_e; K_p$) slopes, as proposed by Jaspart (Jaspart, 1991). Numerical and experimental design resistance predictions are generally under 10% error range. Analytical predictions provide expectedly conservative results.

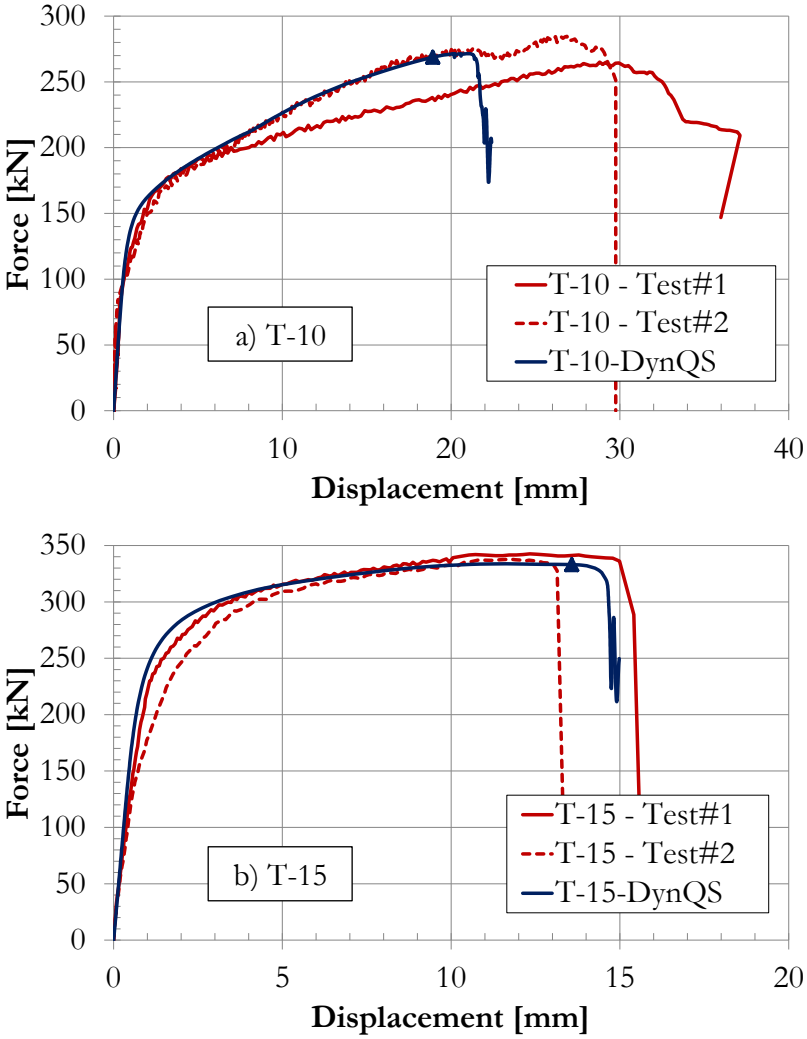

Figure 5.1 – Force displacement curve for monotonic loading: Numerical versus experimental results.

Comparing the global $F-\delta$ response from both T-stubs, it can be observed that T-15 exhibits stiffer behaviour, higher ultimate strength but reduced displacement capacity. Although both specimens were bolted with the same M20 (8.8) bolt and both failed through the bolt's rupture, the ultimate strength of T-10 is 84% from T-15's, due to the higher shear stress level developed in T-10's bolt. The model is able to predict the collapse with reasonable agreement for both thicknesses. It is verified that T-10 is able to reach around 30 mm of displacement, whilst T-15 merely reaches half of that value. The triangular marker in Figure 5.1 identifies the last increment before damage is detected in the bolt, and it will be treated as a reference increment for the study of the strain patterns presented in Figure 5.2.

Table 5.1 – Comparison of values for Design Resistance, Initial Stiffness, Post limit Stiffness and Displacement Capacity obtained with the Eurocode, Experimentally and Numerically

		Design Resist. [kN]	Initial Stiffness [kN/mm]	Post limit Stiffness [kN/mm]	Displacement Capacity [mm]
		20ºC	20ºC	20ºC	
T-10	Analytic – EC3	101.6	130.4	--	--
	Experimental	182.4	171.4	3.1	32.0
		158.5	179.1	6.8	29.5
	Numeric	161.6	170.6	6.2	21.1
T-15	Analytic – EC3	212.7	336.2	--	--
	Experimental.	300.8	261.0	3.9	13.0
		291.0	271.0	4.7	15.0
	Numeric	294.0	246.0	4.6	14.5

The analysis of the equivalent plastic strain patterns (PEEQ) in Figure 5.2a) shows the development of two plastic hinges per T-stub leg, for T-10, while for T-15 only the one next to the weld toe is completely developed; this is in accordance with the Eurocode 3, part 1.8, where the plastic failure modes are *mode 1* and *mode 2*, respectively (EN 1993-1-8, 2005). Figure 5.2b) compares the damage scalar variable (SDEG) for the reference time increment. Next to the weld toe, T-10 exhibits SDEG values around 4 times higher than the ones in T-15; this is in agreement with experimental evidences, where cracks were detected prior to the bolt rupture in the heat affected zone on T-10-Test#1 specimen (followed closely by the numerical response in Figure 5.1) and not on the T-10-Test#2 and T-15 specimens (Figure 5.2c). Figure 5.3 depicts an increment after the reference time increment, where the bolts are unable to hold the applied loading and some elements have already reached a level of damage of D=1, and thus have been deleted from the mesh. Separation of the bolt in two different bodies is clear for both models; model T-15 presents accurate prediction of the displacement capacity – Figure 5.1. However, for T-10 specimen, the initial cracks detected in the heat affected zone inducing flange fracture previous to the bolt failure (Figure 5.2c) are not observed in the numerical model. This difference may be attributed the material model adopted for the welded zone, which is the same as the one considered for the base material.

T-10 – M20 (8.8) δ = 18.91 mm; F = 268.74 kN Mode 1	T-15 – M20 (8.8) δ = 13.57 mm; F = 333.08 kN Mode 2
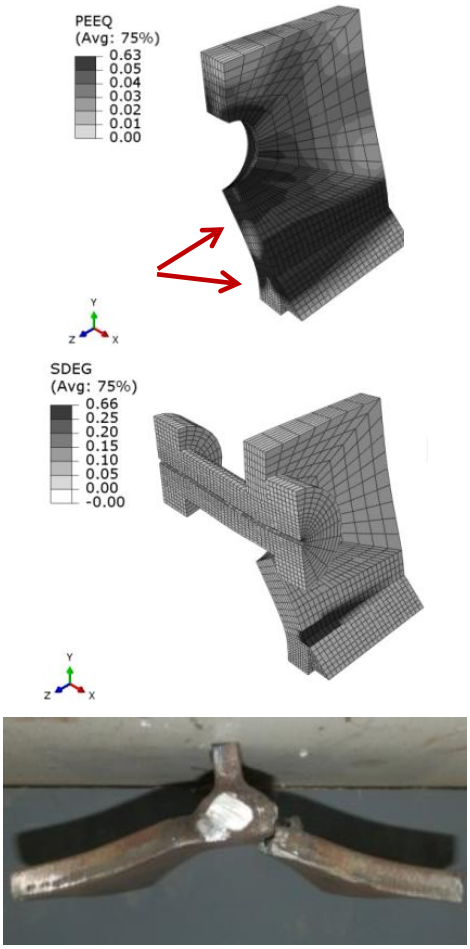	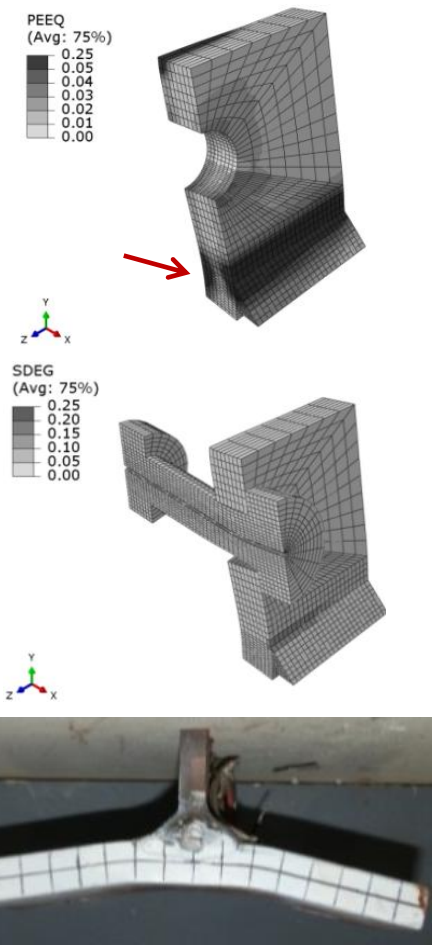

Figure 5.2 – a) Equivalent plastic strain patterns (PEEQ); b) Damage scalar variable (SDEG) [-] for the reference time increment identified in Figure 5.1; c) experimental failure modes (T-10-Test#2; T-15-Test#1) (Barata *et al.*, 2013).

T-10 – M20 (8.8)	T-15 – M20 (8.8)
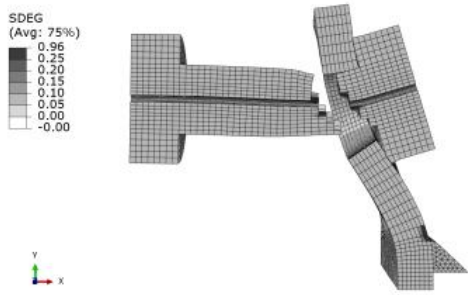	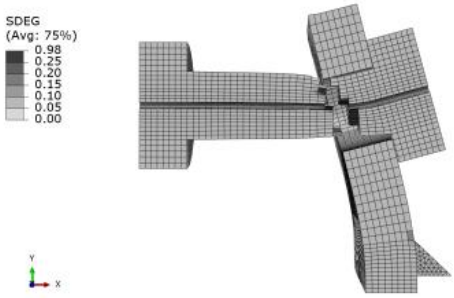

Figure 5.3 – Damage scalar on T-10 and T-15.

5.2 Validation under impact loading

5.2.1 Load application procedure

The numerical validation under impact loading considers only results for T-10 specimen, for two different load levels input on the experimental tests according the experimental layout described in Section §4: gas pressures of 120 Bar (Impact #1 of T10-D120-160) and 160 Bar (Impact #1 of T10-D160) (Barata *et al.*, 2014b). Each load level induces a transient displacement curve represented in Figure 5.4; the maximum displacement values are reached in approximately 80 miliseconds. These experimental displacement fields are applied as a boundary condition in the "*pull out surface*" of the numerical model (Figure 4.9) and the generated reaction forces on the "*fixed surface*" extracted.

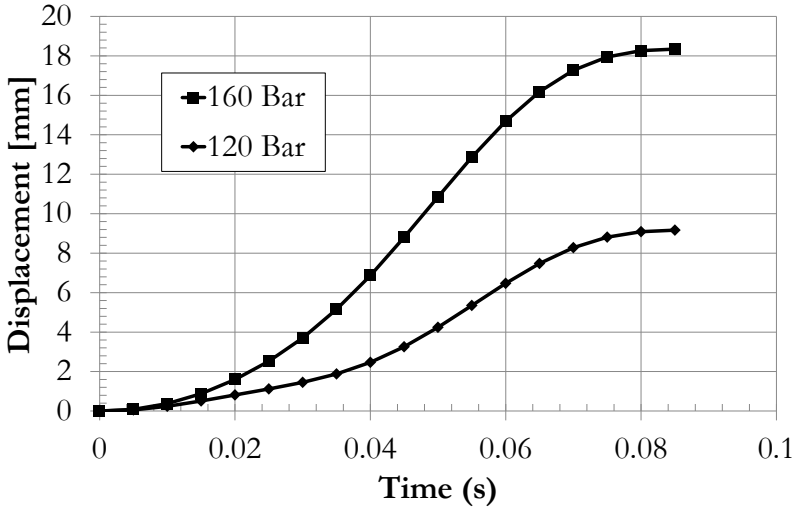

Figure 5.4 – T-stub displacement curves measured experimentally and used for displacement based dynamic loading application in the FEA.

5.2.2 Numerical versus experimental results

Figure 5.5 and Figure 5.6 compare the T-10 force-displacement (F-δ) response subject to quasi-static (blue dotted line – numerical curve) and rapidly applied dynamic loads with different intensity (red dotted line – numerical curve and red dashed line – experimental curve). The close agreement between experimental results and numerical responses confirms that the model is adequate to describe the behaviour of the tensile component subject to impact loadings, and, particularly, that the Johnson-Cook material model with the dynamic increase factors described previously (see Figure 3.4) provide accurate stress enhancement. Figure 5.7 illustrates the pattern of the strain rate (ER), ranging from 1/s to 3/s in the plastic hinge developed next to the weld toe, corresponding to DIFs of 1.27 and 1.31 (see

Figure 3.4), while Figure 5.8 presents superposition of quasi-static and dynamic loading levels of 120 and 160 Bar obtained numerically. It can be observed that the elastic stiffness remains unchanged for all loading schemes, as the steel's elastic modulus introduced in the numerical models is the same for both quasi-static and dynamic situations, accordingly to Section 3. For the same displacement instant, the strain rates developed are similar for both dynamic loading (Figure 5.7) inducing the same dynamic increase factors for the stress enhancement; the F-δ flows are therefore, similar for both numerical dynamic responses up to the end of 120 Bar response (Figure 5.8). The markers in Figure 5.8 represent the plastic resistances of the T-stub: $F_{Rd,\ quasi\text{-}static}$ = 161 kN and $F_{Rd,\ 120Bar}$ = $F_{Rd,\ 160Bar}$ = 195 kN; corresponding to an enhancement of +21% of the plastic resistance due to the strain rate effects. No failure has been observed neither in the experimental tests nor the numerical models.

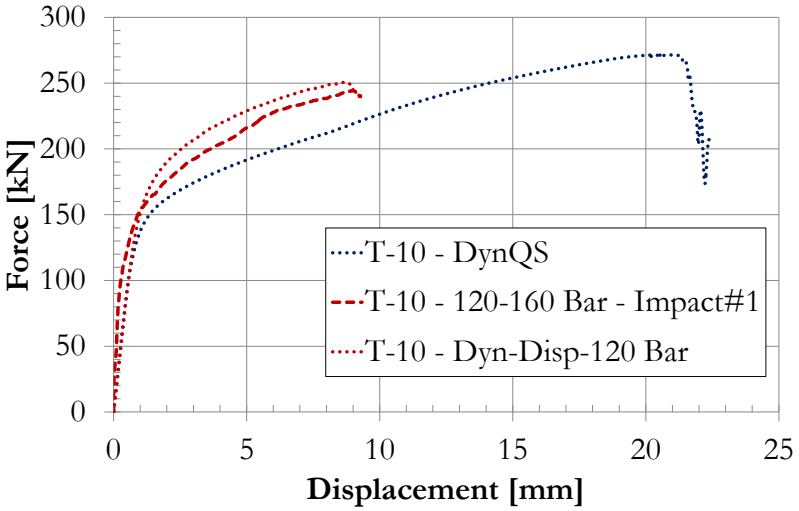

Figure 5.5 – T-10 F-δ responses: Experimental 120 Bar loading Vs. numerical quasi-static and 120 Bar loading.

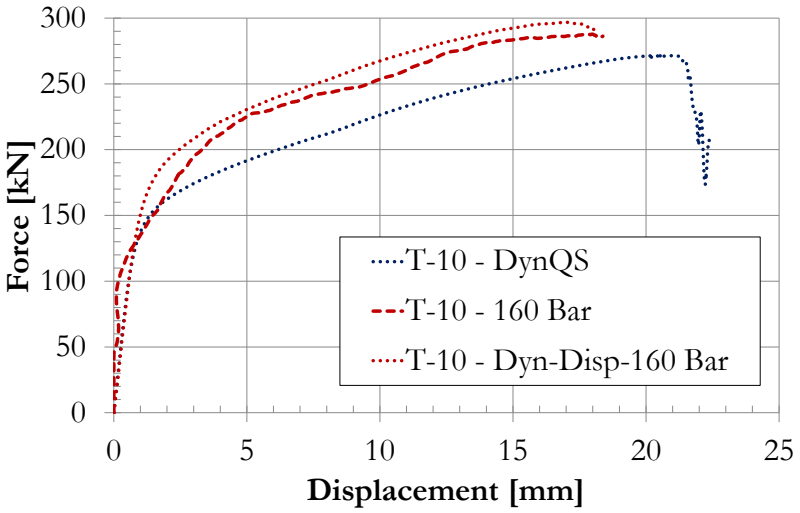

Figure 5.6 – T-10 F-δ responses: Experimental 160 Bar loading Vs. numerical quasi-static and 160 Bar loading.

Dynamic – 120 Bar δ = 1.76 mm F = 184.0 kN	Dynamic – 160 Bar δ = 1.71 mm F = 184.5 kN
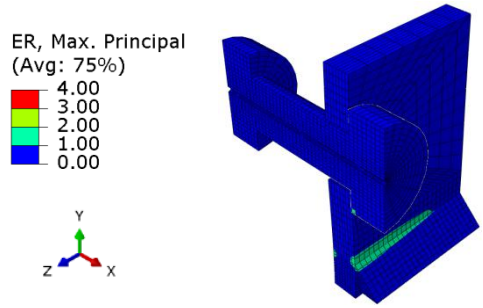	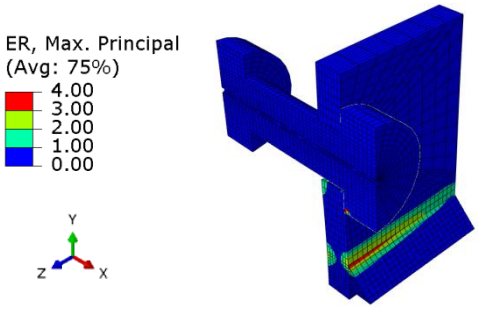

Figure 5.7 – Strain rate for loadings a) 120 Bar and b) 160 Bar for a global T-stub displacement of δ = 1.7 mm.

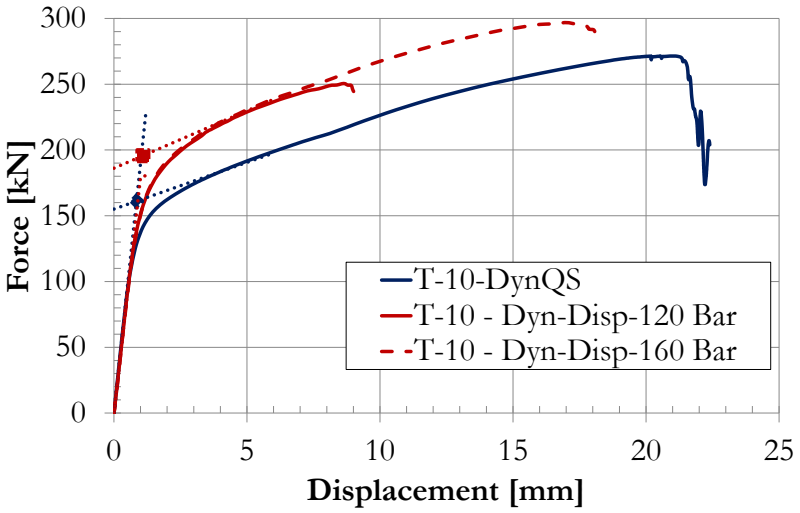

Figure 5.8 – T-10 Numerical predictions;
Quasi-static, 120 Bar & 160 Bar.

For a time step near the end of the analysis (δ = 18 mm approximately), Figure 5.9 compares the equivalent plastic strain (PEEQ) patterns for the quasi-static and dynamic (160 Bar) response; it can be observed that for both situations two plastic hinges are developed per flange leg, consistently with the plastic failure mode type 1 predicted by the Eurocode 3, part 1.8 (EN 1993-1-8, 2005). However, in the dynamic case, the plastic hinges are slightly underdeveloped and higher strains are required in the bolt to meet the same deformation level (Figure 5.9b). As the increase of the strength is greater in the flange ($DIF_{flange} \approx 1.3$) rather than the bolt (maximum $DIF_{bolt} = 1.1$), stiffer plastic and failure modes are triggered.

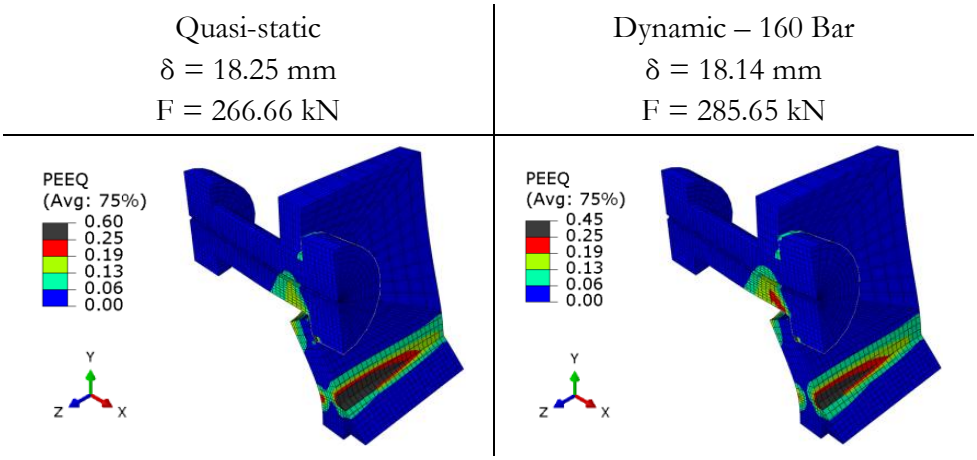

Figure 5.9 – Equivalent strain patterns (PEEQ) [-] – a) Quasi-static Vs. b) Dynamic 160 Bar.

5.3 Behaviour under impact loading – Parametric studies

5.3.1 Load application procedure

Parametric studies regarding the maximum applied load (P), the load application time (t_1) and the thickness of the T-stub flange (t_f) are conducted. The main purpose is to verify how the maximum resistance and post limit flow are affected by the dynamic load parameters, owing to the fact that the material's stress-strain relationship is itself dependent on the applied strain-rate, and, therefore, a function of the applied load.

Figure 5.10 presents the "*rectangular*" *sudden* dynamic load application scheme applied: loading is set to rise to its peak in an application time (t_1), remaining constant during a time interval equal to the application time ($\Delta_{t0 \rightarrow t1} = \Delta_{t1 \rightarrow t2}$). Reference time of t_1 = 10, 1, 0.5 seconds and t_1 = 80 and 20 milliseconds are assessed for peak loads P = 1x, 2x and 4x the maximum static resistance of the specimen ($F_{máx(T\text{-}10)}$ = 277 kN; $F_{máx(T\text{-}15)}$ = 334 kN).

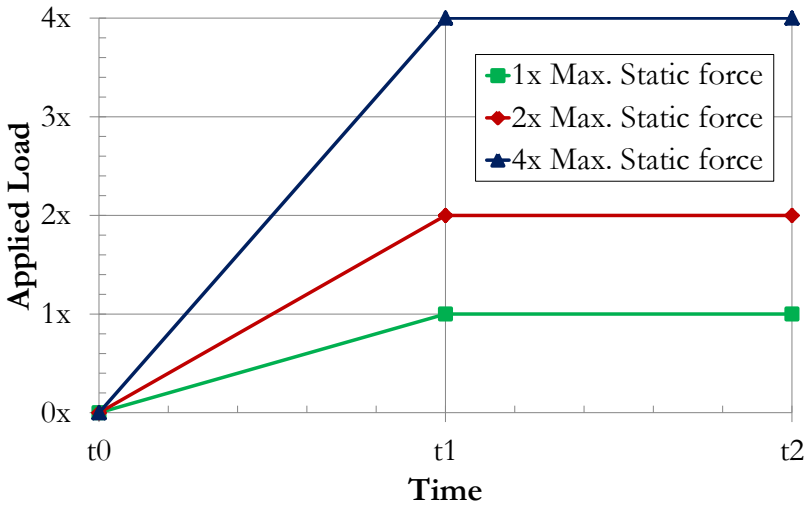

Figure 5.10 – Dynamic load application scheme.

5.3.2 Influence of the maximum applied load

Studies assessing the effects of the dynamic loading start with a verification of the effects for a peak load equal to the maximum static resistance are made ($P = 1 \times F_{máx}$). The load is applied in an application time t_1 = 20 ms, consistent to literature suggestion (Chang & Tyas, 2011). The static results vs. dynamic results are presented in Figure 5.11; both T-stubs are able to resist their static failure load when it's applied in a short period of time as no signs of failure are observed under dynamic loading. The effects of the increase of the strain-rates can be observed through the increase in the plastic resistance. In addition, for the same applied load, the maximum deformation decreases in the dynamic cases.

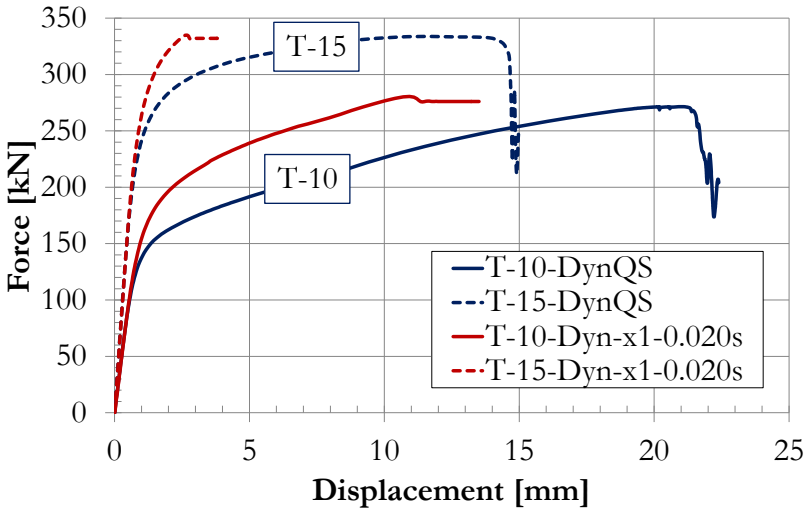

Figure 5.11 – Static results vs. Dynamic results for 1.0x the static resistance load applied in 20 ms

For the studied geometries (T-10 and T-15), the following values are considered for the applied loading: case 1A) P = 1×$F_{máx.}$; case 1B) P = 2×$F_{máx.}$ and case 1C) P = 4× $F_{máx.}$; the application time is the same in all cases (t_1 = 20 msec.). Figure 5.12 compares the static response with the dynamic responses of both reference T-stubs. Despite the response enhancement observed from quasi-static to dynamic analysis, different values of the dynamic peak load (P) seem to have no influence in the T-stub global behaviour. However, specific observations are reported:

i. The effects of the increase of the strain-rates can be observed through the increase in the plastic resistance: 21% and 9% for T-10 and T-15, respectively.
ii. Ultimate failure load is increased over 15% for both T-stubs (16% and 18.6% increase for T-10 and for T-15, respectively). The ultimate failure mode remains as the bolt rupture, therefore dependant on the bolt resistance capacity, justifying why this increase is similar for both models.
iii. The rotation capacity of T-10 is reduced when subject to dynamic loads due to the lack of development of the plastic hinge next to the bolt. Consequently the bolt is required to deliver higher strains leading to a reduction in the displacement capacity.

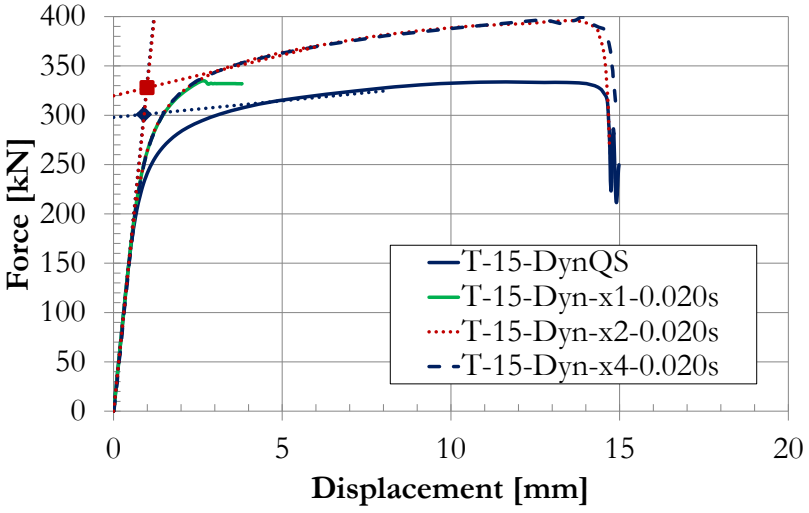

Figure 5.12 - Force versus displacement curves for a) T-10 and b) T-15 subject to static and dynamic loads.

For the T-stub T-10, Figure 5.13 compares the Von Mises stress pattern obtained from the static analysis and the dynamic analysis considering the same T-stub deformation level of 15.4 mm: stresses above 950 MPa (f_{ub}) on the bolt and higher stress level on the flange next to the weld toe are observed in the dynamic analysis, owing to the higher level of resistance

capacity, as demonstrated in Figure 5.12. Analysis of the equivalent plastic strain patterns on the flange shows that the dynamic case activates higher plastic modes once only one plastic hinge per leg is fully developed, in contrast with observations from the quasi-static case where a second plastic hinge near the bolt is established.

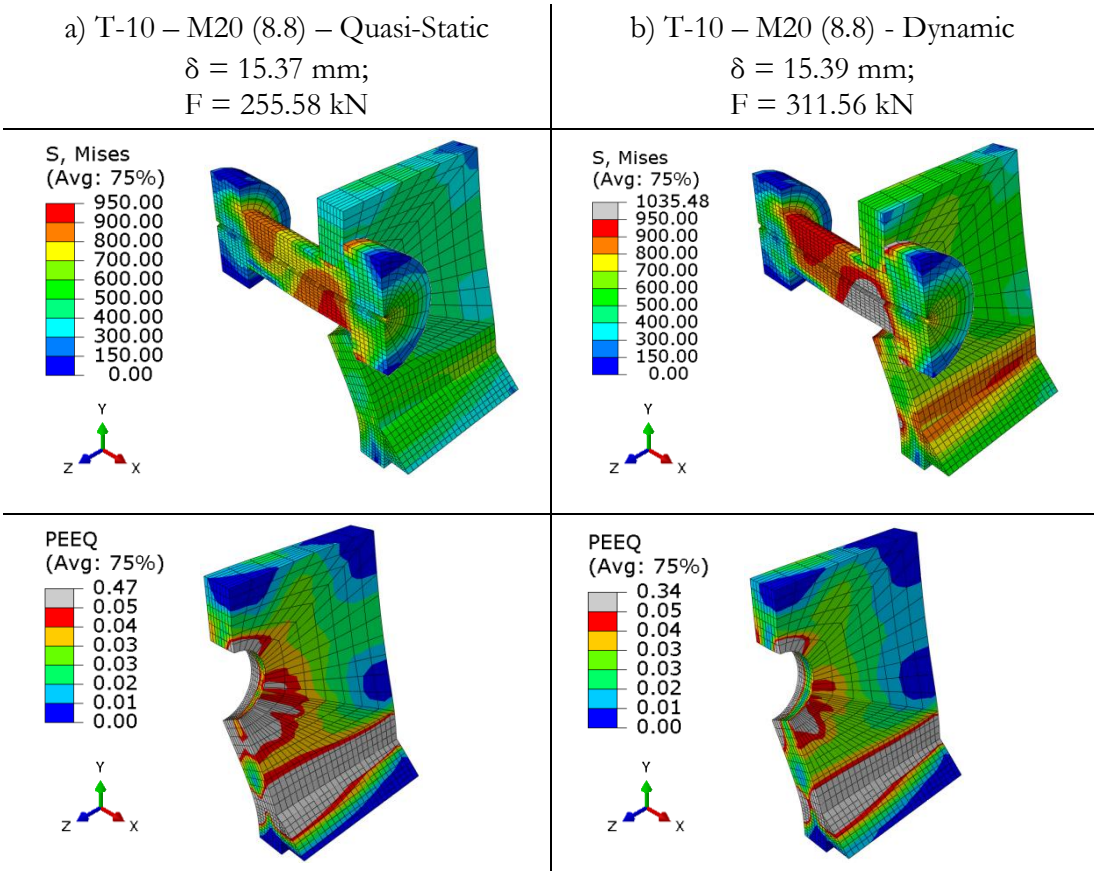

Figure 5.13 – Von Mises (S, MISES) [MPa] stress patterns and equivalent plastic strain patterns (PEEQ) for T-10: a) static loading b) dynamic load

5.3.3 Assessment of application time influence

This section concerns the assessment of the effects of the loading application time (t_1). The following application times are considered: t_1 = 10, 1 and 0.5 seconds and also t_1 = 80 and 20 milliseconds; the applied load magnitude is the same for all cases: $P = 4 \times F_{máx}$. The loading application times are chosen to demonstrate the effects of subjecting the T-stub to different strain rate levels; For T-stub T-10, Figure 5.14 demonstrates that as the application time gets smaller, the force-displacement response is enhanced. The numerical response used to validate the dynamic experimental results from Impact #1 – D160 Bar is similar to the response from case 2C) t_1 = 500 msec. The 80 millisecond response demonstrates that,

despite having the same application time as in the experimental tests, with an increased loading magnitude, the response can yet be enhanced.

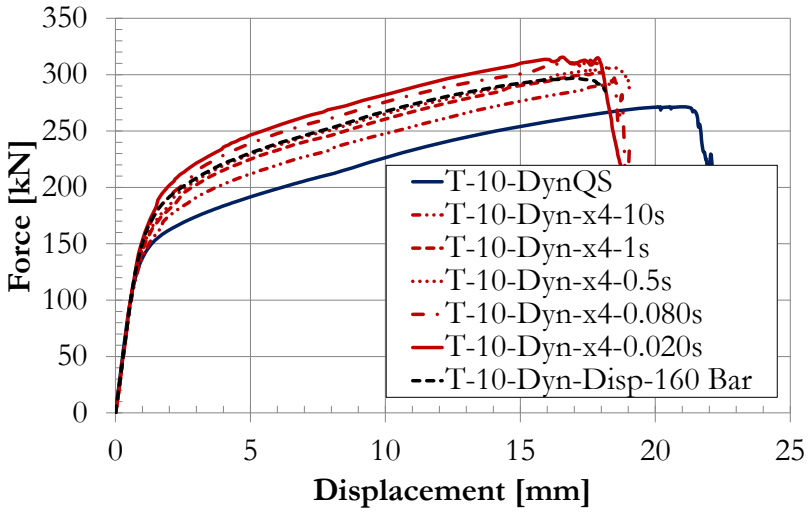

Figure 5.14 – Force versus displacement curves for different applications times (t_1).

5.3.4 Influence of the thickness of the T-stub

This section concerns the variation of the flange thickness of the T-stub (t_p): two additional flange thicknesses are considered: t_f = 8 mm and t_f = 40 mm; the application time and the applied load are the same in all cases: t_1 = 20 msec. and P = 4× $F_{máx.}$. Although t_f = 40 mm does not reproduce a usual T-stub geometry, it has been chosen to verify the response of stiffer plastic failure modes (*mode #3*). Figure 5.15 presents the corresponding force-displacement responses; it is observed that plastic resistance is increased by 5% for T-40, while for T-8 the plastic resistance is increased by 20% due to the strain-rate effects on the materials' hardening. For T-8's F-δ response, failure cannot be observed for static solicitation as the damage is being developed in the flange and convergence difficulties lead to an early stop of the analysis. However, in the dynamic case the ultimate failure is the bolt rupture with elevated damage in the flange next to the weld toe. For T-40, the collapse is the bolt's failure in both cases; oddly enough, the dynamic case exhibits a slight (and rather meaningless) increase of the displacement capacity.

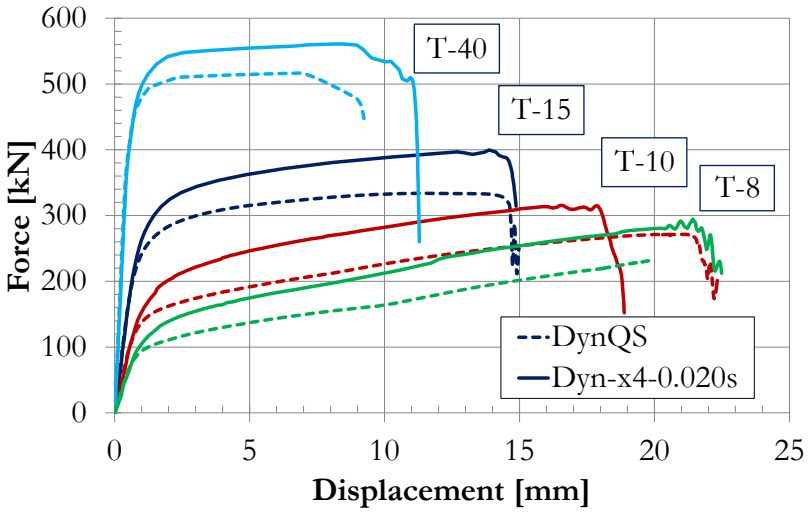

Figure 5.15 – Force versus displacement curves for different T-stubs thickness (t_p).

Two finite elements are chosen to plot of equivalent plastic strain (PEEQ) versus Von Mises stresses (Figure 5.17) and the PEEQ versus the measured strain-rate (ER) (Figure 5.18). Finite elements are chosen in zones where plasticity may firstly occur: in the interface of the flanges for the bolt; and in the plastic hinge formation zone in the flange (Figure 5.16).

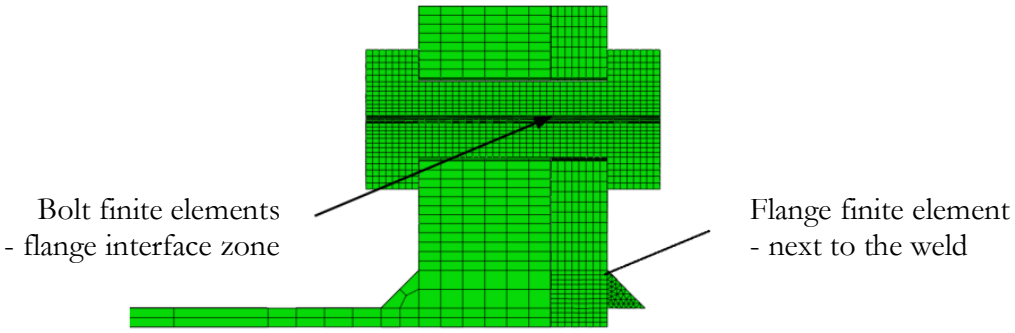

Figure 5.16 – Picked finite elements

Figure 5.17 and Figure 5.18 compare the picked finite element in the bolt (red colored lines), the finite element in the plate (blue lines) for the thicknesses of T-10 (solid lines) and T-40 (dotted lines). The absence of a **blue dotted line** in both figures shows that the T-40 plate finite element does not enter its plastic phase (Figure 5.17) therefore remaining within the elastic range during which strain variability is small (Figure 5.18).

On the other hand it is verified that the strain rate is higher in the bolt for T-40 rather than in T-10. Figure 5.17 however, shows that the computed stresses in the bolt element are roughly the same for both thicknesses.

In Figure 5.17, it may also be observed that the particular element chosen from the flange of T-10 (blue solid line) has already lost its load carrying capacity. The element reaches its peak for a PEEQ value around 0.14 and thereafter begins its softening phase, driven by the damage evolution behaviour presented previously, which, in the case of S355 steel, requires the element to develop a damaged effective displacement ($\bar{u}^{pl}$) of 1.5 mm before it is removed from the mesh. This demonstrates that the finite element model developed elevated damage on the flange next to the weld toe, accordingly to the cracks observed for T-10 test specimen, yet the ultimate failure has been the bolt.

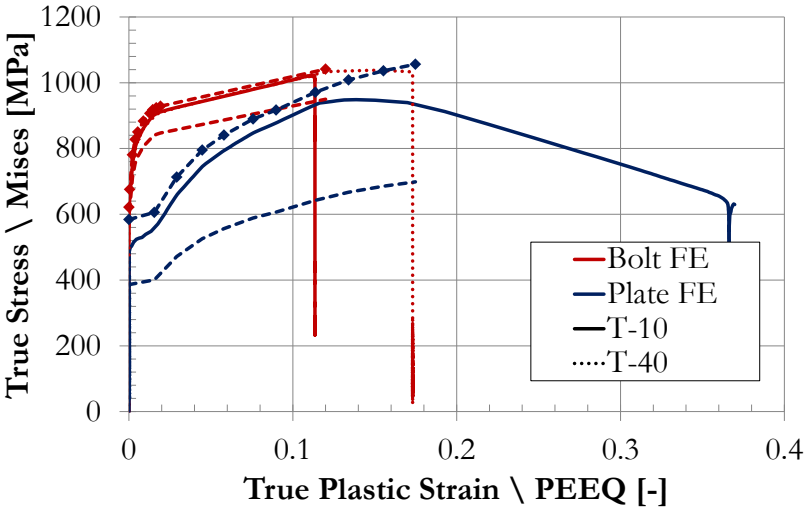

Figure 5.17 – Computed stress-strain relationship Vs. material properties included in the numerical model

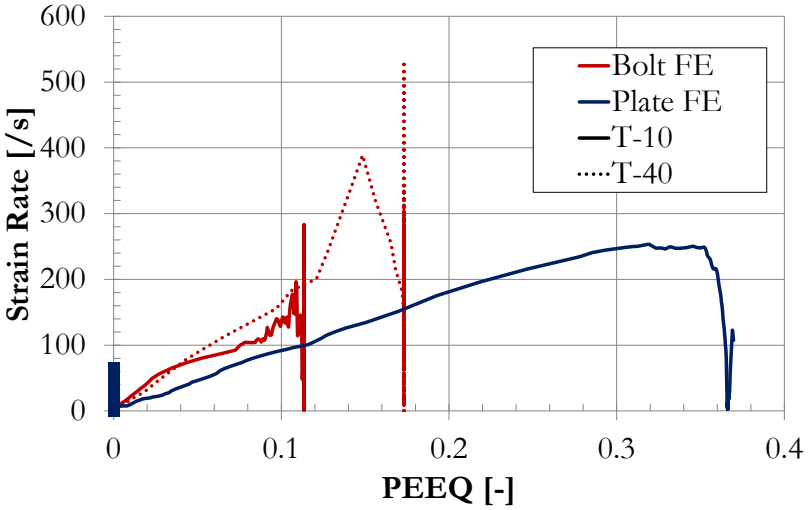

Figure 5.18 – PEEQ vs. strain rate for the picked finite elements

5.4 Concluding remarks

Current chapter demonstrates that the finite element model is accurate in describing the non-linear behavior of T-stubs under quasi-static and short transient loadings. Under quasi-static conditions, the input damage model proved accurate in delivering the ultimate displacement capacity through the bolt rupture. The parametric study conducted under dynamic loading concerning the load application time, load magnitude and T-stub flange thicknesses ranging from t_f = 8 to t_f = 40 mm showed that: i) the T-stubs are able to resist the maximum strength observed for quasi-static conditions with reduced displacement, due to the material strength enhancement provided by the elevated strain rates developed; ii) more flexible T-stubs have larger increase in the strength enhancement, yet a reduction in the displacement capacity is observed for T-10; iii) different loading magnitudes applied in the same 20 milliseconds delivered similar response while considering different loading application times (ranging from 10 seconds to 20 milliseconds) demonstrated a resistance capacity enhancement for shorter application times; and iv) stiffer plastic failure modes are triggered under dynamic condition whilst T-stubs following "*mode 3*" for static conditions are unable to take advantage of the strength increase in the flange .

6. T-STUB BEHAVIOUR UNDER IMPACT LOADING – ANALYTICAL APPROACH

6.1 Simplified evaluation – EC3 – Part 1.8

Based on the simplified procedure for the evaluation of resistance and stiffness of the T-stub described in Eurocode 3, Part 1.8, (see Section 2.2) this section concerns the implementation of elevated strain rate effects through the enhancement of steel's and bolt's strengths with dynamic increase factors (DIF), for the calculation of the T-stub resistance when subject to rapidly applied dynamic loads.

From eq. (1) to (3) in Section 2.2, it can be observed that the design resistance from *Mode Type 1* is merely affected by the elastic strength of the steel flange (f_y), whereas *Mode Type 3* is directly affected by the bolt strength (f_{ub}); therefore any DIF applied to the steel flange or the bolt within these modes, respectively, will result in a direct increase of the design resistance. *Mode Type 2*, on the other hand, is not directly affected by an increase in the elastic strength of the steel flange or the bolt strength, but it depends on both simultaneously. Thus, the resistance of the T-stub under rapidly applied dynamic loads is the minimum value obtained from eq. (1) to (3), but f_y and f_{ub} in eqs. (4) and (5) should be replaced by $f_{y,d}$ and $f_{ub,d}$, respectively, to account for the strain rate effects:

$$f_{y,d} = DIF_{steel} \cdot f_y \tag{14}$$

$$f_{ub,d} = DIF_{bolt} \cdot f_{ub} \tag{15}$$

Using this simplified evaluation, the effect of the strain rate on the T-stub failure modes is assessed. Table 6.1 depicts the influence of increasing *DIF* values in the elastic strength of

the flange's steel in the increase of the design resistance of the T-stubs, assuming a constant *DIF* for the bolt (DIF_{bolt} = 1.1); failure modes #1, #2 and #3 are covered by considering multiple T-stub thicknesses ranging from 10 to 30 mm, whilst bolts M20, class 8.8 are used. The shaded area in Table 6.1 denotes the T-stubs with a failure *Mode Type 2*. It can be observed that:

- With increasing DIF_{steel} less ductile failure modes are activated; for instance, for t_f = 25 mm, *Mode Type 2* is obtained for DIF_{steel} = 1 and 1.1; however, for higher values, *Mode Type 3* will appear. The same is observed for others T-stubs: t_f = 20 mm changes from *Mode Type 2* to *Mode Type 3* for DIF_{steel} = 1.8, and t_f = 10 mm changes from *Mode Type 1* to *Mode Type 2* for DIF_{steel} = 2.2.
- For the same failure mode, stiffer T-stubs exhibit higher increment for the same DIF, as exemplified in **bold** for DIF_{steel} = 1.5 (an increase of 15% is obtained for t_f = 15 mm, while for t_f = 20 mm an increase of 22% is noted).
- Increasing DIF in the steel flange doesn't affect T-stubs following *Mode Type #3*.

Table 6.1 – Increase of the design resistance for different thicknesses and DIF_{steel} on the T-stub flange

Flange thickness [mm]		**10**	**15**	**18**	**20**	**25**	**30**
Failure mode		#1	#2	#2	#2	#2	#3
Design resistance [kN] (DIF_{bolt} = 1.1)		96	207	235	256	319	345
DIF_{steel}	**1**	1.00	1.00	1.00	1.00	1.00	1.00
	1.1	1.10	1.03	1.04	1.04	1.06	1.00
	1.2	1.20	1.06	1.08	1.09	1.08	1.00
	1.3	1.30	1.09	1.11	1.13	1.08	1.00
	1.4	1.40	1.12	1.15	1.18	1.08	1.00
	1.5	1.50	**1.15**	**1.19**	**1.22**	1.08	1.00
	1.8	1.80	1.24	1.31	1.35	1.08	1.00
	2	2.00	1.30	1.39	1.35	1.08	1.00
	2.2	2.14	1.37	1.46	1.35	1.08	1.00

6.2 Review of Yu's model

Yu and co-authors (Yu *et al.*, 2009) developed an alternative analytical procedure to capture the behaviour of end-plate joint under large deformations. One of the main motivations to develop such model was the study of joints under elevated temperatures conditions; in this situation, semi-rigid joint's ductility capacity and the failure mode are required to establish

the structural behaviour, as opposed to the requirements of initial stiffness and plastic resistance for common design situations at ambient temperature. The model consists in deriving the behaviour of simple yield-lines, which take material hardening into account, and use them as basic units to describe the response of end-plate joints.

Considering the T-stub model as a simplification of the behaviour of end-plate joint, the authors assessed the capabilities of the analytical procedure to describe its force-displacement response $(F-\delta)$ by establishing yield-lines where plastic hinges (W_{PH}) are usually developed (Figure 6.1): W_{PH1} – next to the weld toe and W_{PH2} – in the bolt line. The model is solved following the virtual work's principle of keeping the strain energy a minimum (equation (16)).

$$F.\delta = W_{PH1} + W_{PH2} + W_{bolt} \tag{16}$$

Figure 6.1 presents the yield line model scheme of half the T-stub. Once again, 3D effects are taken into account based on the effective width (yield line). The model was found to be most appropriate for T-stubs with smaller thicknesses in which the bolt is able to effectively hold down the plate both in the edges and in the middle (Yu *et al.*, 2009). The model was validated against experimental and numerical data available from Bursi and Jaspart's (Bursi & Jaspart, 1998), Girão Coelho's (Girão Coelho, 2004) and Spyrou's (Spyrou, 2002), and it was used to predict the behaviour of flush end-plate joints by adding the effects of the several appearing yield lines. The bolt is represented by a spring with a similar strain hardening condition up to the bolt's peak force. A post-peak behaviour simulating the gradual necking and its progressive degradation, important at elevated temperatures, was incorporated but bolt bending remains unaccounted for.

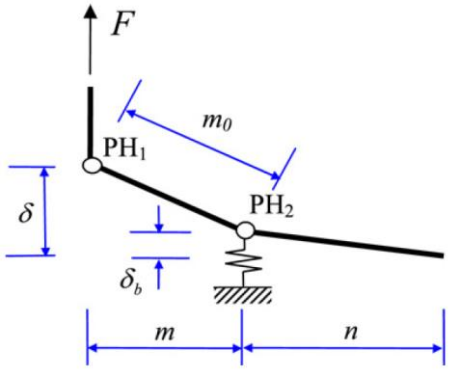

Figure 6.1 – Yield line model scheme of half the T-stub 0

The work for each plastic hinge is obtained by integrating the bending moment over the rotation, considering a three-phase elasto-plastic material model in Figure 6.2b), and a cross-section curvature as a function of the maximum strain in the cross-section; the three curvature diagrams presented in Figure 6.2a) are considered. The size of each plastic hinge is dependent on the parameter k describing the relative dimension of the plastic hinge length to the plate thickness; $k = 2$ has been conservatively adopted by Yu (Yu *et al.*, 2009).

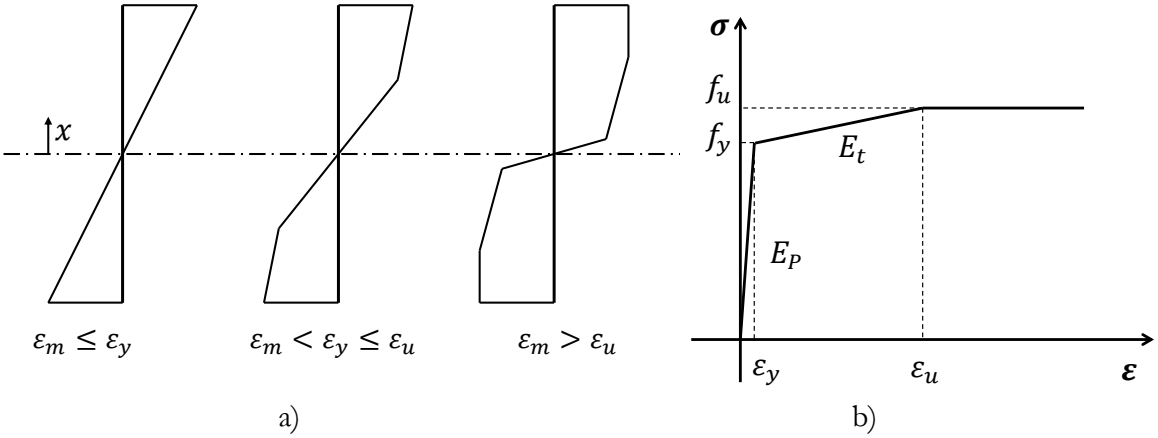

Figure 6.2 – a) Section stress distributions; b) tri-linear material model (Faella *et. al.,* 2000).

6.2.1 Analytical approach to evaluate the non-linear dynamic response of T-stubs

The studied analytical procedures are exemplified for the T-stub geometry presented in Chapter 4.3, and their results are compared with the experimental and numerical results presented in the previous Chapter. The geometrical data and the applied loading considered here correspond to the data introduced in the numerical model. The multi-linear curve describing the material properties considered in the numerical models is simplified for the analytical procedures: i) for the simplified evaluation (EC3, Part 1.8), only the elastic modulus (E) and strengths (f_y for the steel flange and $f_{u,bolt}$ for the bolt) are required; ii); for the non-linear approach following Yu's model, tri-linear curves are established (Figure 6.3) for the quasi-static case and enhanced with a calculated DIF to obtain the dynamic one.

The proposal to include elevated strain rate effects requires the introduction of a time variable in order to compute strain-rate values. The basic assumption is that the total displacement for calculation occurs in a given amount of time. The procedure is summarized in the flowchart of Figure 6.4: firstly, it is assumed that a total displacement (δ) occurs in a given total amount of time (Δt). Then, the analysis is divided in small steps by linearly

discretizing δ and Δt in the number of computed increments (n), thus establishing relationship between a step's displacement (δ_i) and the step time (Δt_i). This stepwise development allows the computation of the induced strain rate on each step ($\dot{\varepsilon}_i$), by calculating the additional rotation required to meet equilibrium (equation (6)), and the updated maximum strain. The added strain for the current step ($\varepsilon_{m,(i)}$) is assumed to be developed the calculated step time (Δt_i), from which point on, the strain rate and respective dynamic increase factor to be applied can be easily obtained. A different DIF for each increment ($DIF_{step,i}$) is calculated and applied in accordance with Jonhson-Cook model, equation (6).

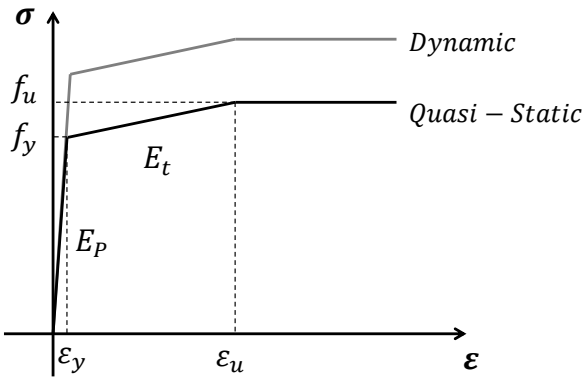

Figure 6.3 – Tri-linear material description used in the non-linear approach.

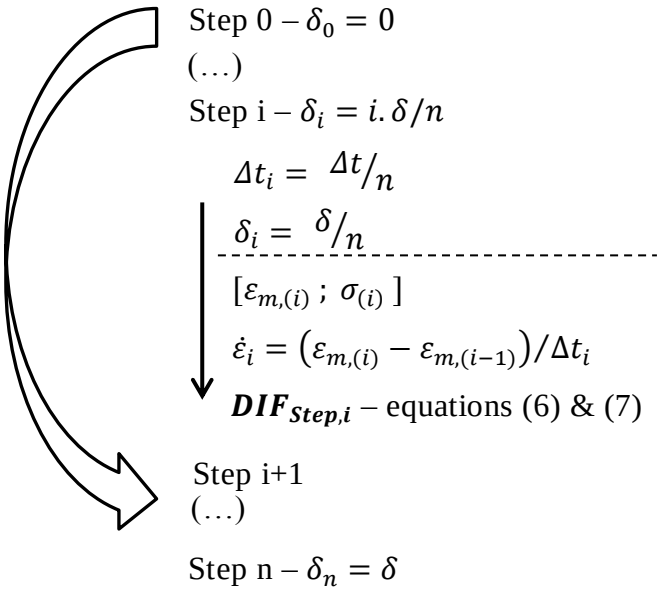

Figure 6.4 – Application of strain rate effects – Flowchart

6.3 Results and Discussion

6.3.1 T-stub under quasi-static loading

The material properties defined in Table 6.2 are established based on the quasi-static tests coupon mentioned previously and are used to compute the analytical models response.

Table 6.2 – Material properties included in the analytical procedure.

	E [GPa]	Et [GPa]	f_y [MPa]	f_u [MPa]	ε_y [10^{-3}]	ε_u [10^{-3}]
Steel S355	205.5	112.0	385	588	1.87	20
Bolt (8.8)	213.5	156.3	518.4	712.8	3.37	15

Figure 6.5 presents the comparison of the response obtained experimentally (Barata *et al.*, 2013) (solid green line), numerically (dotted blue line), and from application of the analytical methodology proposed by Yu (dashed red line). Plastic resistance predictions following the Eurocode 3, part 1.8 (EN 1993-1-8, 2005), are represented by the horizontal lines, while the numerical peak load from Yu model is identified by the red triangular markers.

It is observed that the analytical model it is able to provide approximate prediction of the $F - \delta$ response. For T-10, the analytical model provides rather conservative prediction of the peak load, whereas for T-15, the prediction of the peak load is accurate. The negative stiffness after the peak load is a result of the necking and progressive degradation routine implemented on the bolt element.

The progressive degradation of the bolt aims at the description of the weakening of the bolt after its ultimate strength has been reached. This bolt's post peak behaviour is derived after test observations that at elevated temperatures a gradual necking of bolt's shank is developed, reducing the effectiveness of the bolt to hold down the plate thus hindering the development of prying forces at the free edge of the plate. However, at ambient temperatures, the bolt usually fractures abruptly soon after the peak strength has been reached and no weakening of the bolt is detected; therefore the bolt's displacement should be monitored and a failure criterion should be established and added to this analytical procedure.

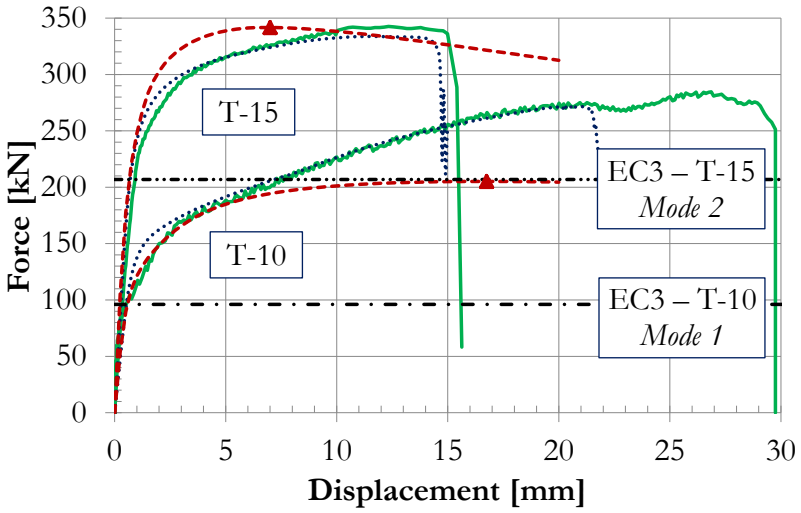

Figure 6.5 – T-stub monotonic $F-\delta$ response for the T-stub specimens T-10 and T-15

6.3.2 T-stub under impact loading

The response obtained following the implemented analytical model is compared with i) results from EC3 - Part 1.8 and ii) non-linear dynamic finite element predictions calculated with ABAQUS software (Abaqus, 2011) (described in Chapter 5). Figure 6.6 and Figure 6.7 compare the static (solid blue lines) and dynamic (solid red lines) $F-\delta$ analytical responses with the corresponding numerical analyses (dashed lines) and predictions of the plastic resistance following Eurocode 3, Part 1.8 represented by the horizontal lines (dash-point).

Examination of the non-linear analytical curves shows that the improvements introduced in the model enable the computation of strain rate and adoption of dynamic increase factors enhancing the strength of the T-stubs. Small increments of $\delta_i = 0.25$ mm are used to compute the response; for T-10 the same total displacement of $\delta = 18$ mm in $\Delta_t = 80$ ms, as observed in the experimental test *T-10-D160 Impact #1*, is considered. Thus a total of $n = 72$ increments are required for T-10. For T-15 a displacement of $\delta = 20$ mm is considered in the same $\Delta_t = 80$ ms.

For the simplified evaluation global *DIFs* are considered: T-10's flange, $\dot{\varepsilon} = \frac{\delta_i}{\Delta_t} = 18/0.080 = 225\ s^{-1}$ and for T-15 $\dot{\varepsilon} = 20/0.080 = 250\ s^{-1}$, therefore, a $DIF_{steel} \approx 1.5$ might be globally assumed (Figure 3.4) for both thicknesses; for the bolts DIF_{bolt} of 1.1 is assumed.

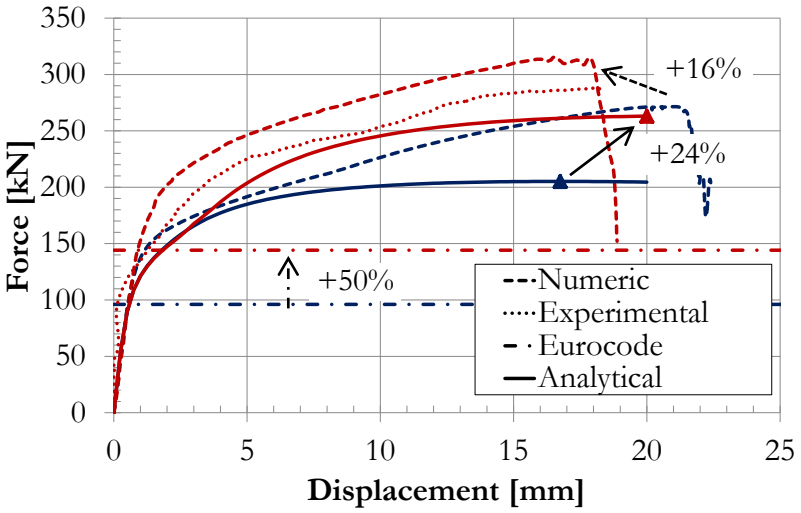

Figure 6.6 – T-10 analytical model $F - \delta$ response

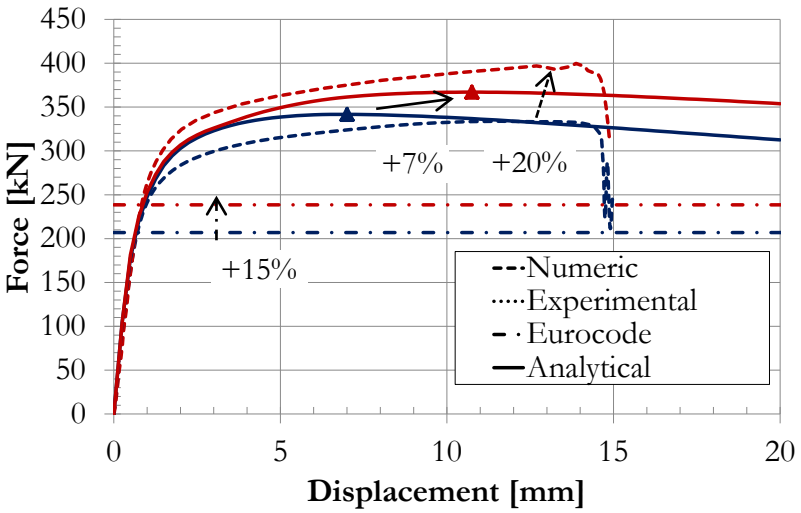

Figure 6.7 – T-15 analytical model $F - \delta$ response.

The plastic failure *Mode Type 1* followed by T-10, produces a dynamic plastic resistance predicted by Eurocode to increase 50 % compared to the monotonic results, whereas in the non-linear analytical procedure only an increase of 28% is reached. For T-15 (*Mode Type 2*) the Eurocode predicts a 15% increase and the non-linear model merely 7%.

Both monotonic and dynamic predictions by the Eurocode provide safe but rather conservative results, especially in what structural over strength capacity assessment for progressive collapse analysis is concerned, since structures may be required to perform in a post-limit regime.

The analytical procedure is able to compute the formed plastic hinges accordingly to the Eurocode's, Part 1.8 plastic failure mode predictions; the stepwise development of the non-

linear analytical model allows the computation of a dynamic increase factor for each step; Table 6.3 presents the average and maximum DIFs computed within the analytical procedure for plastic hinge 1 (PH1) next to the weld toe, for plastic hinge 2 (PH2) next to the bolt line, and in the bolt. It can be observed that the lowest average DIFs are PH2 of T-15 and the bolt on T-10, demonstrating that T-15 improves the strength of only the PH1 and the bolt, and T-10 of both plastic hinges but not the bolt.

The advantage of the analytical procedure, compared to the Eurocode 3, Part 1.8 procedure, is the ability to describe the post-limit behaviour of the $F - \delta$ response, while enhancing its resistance under short transient loads, similarly to what was observed in the numerical models. Once the procedure is programed in a VBA routine, it is quicker to derive the response of T-stubs rather than building a FE model.

Table 6.3 – Average and maximum computed DIF in the analytical procedure.

T-10	PH1	PH2	Bolt
Average	1.38	1.35	1.01
Max	1.38	1.36	1.08

T-15	PH1	PH2	Bolt
Average	1.36	1.02	1.09
Max	1.38	1.35	1.09

6.4 Concluding remarks

The chapter explored the simplified Eurocode evaluation of T-stubs and a non-linear analytical model available in the literature developed by Yu and co-authors (Yu *et al.*, 2009). While the Eurocode approach provides expectedly conservative results in predicting the plastic resistance of T-stubs, the non-linear model is able to describe the hardening behavior: slight over strength is predicted for T-15 whilst for T-10 the response is under predicted.

Both models are improved to account for elevated strain rate effects; in the simplified model the approach has been to directly apply DIFs enhancing the material strength: it is demonstrated that increasing DIFs will deliver stiffer failure modes. For the non-linear model, elevated strain rate effects are accounted for by introducing a time variable in which the load is applied; due to the step wise nature of the model and by linearly discretizing the

load application time, the additional strain required to meet equilibrium at each step is used to compute the strain rate and thus calculate the DIF to be applied. The improvements allowed to describe the strength enhancement behavior observed in the previous finite element models, showing smaller strength enhancement for stiffer T-stubs.

7. CONCLUSION

7.1 Conclusion

The present thesis concerns the non-linear dynamic response of T-stubs under short transient loads. The T-stub model is used in the "component method" to define the behaviour of components able to provide ductility to bolted steel joints; compared to a whole joint, it is a far less complex model, thus suitable for a first approach addressing its behaviour under short transient loads. This thesis deals with this subject by studying the non-linear behaviour of the T-stub model under impact loads by means of a numerical and analytical approach. Firstly, relevant features are explored and incorporated in a numerical model: i) the effects of elevated strain rates on the mechanical properties of the material; ii) a failure criterion to predict the onset of damage; iii) selection of the numerical algorithm to solve the dynamic problem; iv) then, the numerical model is validated against quasi-static and impact loading experimental evidences and v) assessment of parameters that influence the dynamic behaviour of the T-stub are presented; finally, vi) analytical models available in the literature are explored.

A thorough finite element model considering a failure criterion is built and validated against quasi-static and dynamic experimental test results gathered from research project "ImpactFIRE" carried at the University of Coimbra; the results from welded T-stubs with flange thicknesses of 10 and 15 mm (S355) bolted with M20's class 8.8 showed that the numerical model is reliable to predict the force-displacement response, displacement capacity and the resistance. Elevated strain rate effects on the material are considered following the Johnson-Cook law, established considering the results from Split Hopkinson bar tests performed on mild steel specimens.

The advantages of using implicit and explicit methodologies were discussed; taking into account that the analysed models are small, the implicit methodology using the Hilber-

Hughes-Taylor direct integration method providing numerical dissipation, result accuracy check and allowing unconditional time-increment dependency revealed to be most favourable. The use of an explicit algorithm is understood as being attractive for larger and complex models, for allowing general contact definitions, overcoming numerical singularities with ease and reducing computation costs (for large models). Results obtained using the explicit algorithm revealed that greater expertise may be required to obtain a valid solution.

The first dynamic analysis showed that under short transient load regimes the force-displacement response is enhanced due to elevated strain rate effects and that the T-stubs are able to resist the maximum load observed from quasi-static analysis with reduced deformation. A comprehensive parametric finite element study concerning the dynamic response of the T-stub model is presented: the effects of the peak load magnitude, load application time and the flange thickness are assessed. It is observed that the different dynamic loads within the range considered (1x, 2x and 4x times the maximum static resistance within 0.020 seconds) have minor effect on the force displacement response. However, differences in the response are observed when different load application times were considered (10, 1, 0.5, 0.080 and 0.020 seconds) due to the imposed variability in the strain rate. Concerning the thickness of the T-stub flange, it is concluded that the force-displacement enhancement is less noticeable for the stiffer T-stubs, in particular, for those following a failure *mode type 3*. For this failure mode, the resistance is dependent on the bolt and development of elevated strain-rates in the flange is not observed; thus such T-stubs cannot take advantage of an increase in the strength of the flanges.

It has been shown that stiffer and more resistant T-stubs are obtained if the rate of the load is increased. Particularly, a reduction of the displacement capacity was observed for T-10 due to the reduced development of the plastic hinge next to the bolt; this turned a T-stub initially following plastic *mode type #1* under quasi-static conditions to a plastic *mode type#2*, hence, higher strains are developed in the bolt, resulting in an early failure, although the same damage model is implemented for both quasi-static and dynamic situations

The study also addresses analytical approaches available in literature, namely the simplified calculation method available in the Eurocode 3, Part 1.8 and the model derived by Yu and co-authors (Yu *et al.*, 2009) which is able to describe the non-linear post-limit response. It is found that under static condition the model provides conservative results for T-10 and slight

over prediction of T-15 capacity. The models are improved to include elevated strain rate effects.

The stepwise characteristic of the non-linear model allows the computation of the strain rate at each displacement increment by the linear decomposition of a pre-defined total time frame. Application of 18 mm displacement in 80 ms, as recorded during experimental testing, is studied for T-10 while for T-15 a 20 mm displacement is considered; when compared with non-linear dynamic finite-element analyses and experimental responses the models have delivered results on the safe side.

Using constant Dynamic Increase Factors of 1.5 for mild steel and 1.1 for the bolt, the analytical model prescribed in EC3 - Part 1.8 is used to predict of the plastic resistance of T-stubs for short dynamic loading regimes. Conservative values were obtained compared with non-linear dynamic finite-element analyses responses; however, it should be noted that the constant Dynamic Increase Factors used in this procedure corresponds to high values of strain rates (250/s), which will hardly correspond to a real situation in the entire T-stub yield lines, or even during the entire time in which the loading is applied.

7.2 Future work

The T-stub finite element model described in this work has proven to be reliable in the description of the non-linear behaviour of the T-stub's. Yet, improvements can be achieved through further material characterization. For instance, the extent of validation of the implemented the damage model, and particularly the relationship of the triaxial stress state to the equivalent plastic strain for the damage threshold is unsure for other situations and deserves further developments. Deeper understanding of damage models available in the literature (or development of new) establishing accurate behaviour of mild steel with minimum dependency on the finite element size, could enable finite element models to establish a joints ductility with reduced cost. Furthermore, material toughness variability under short transient load could still be important and has not been addressed.

Although the T-stub is understood as the "driving force" for a joint ductility, this should be confirmed with full scale joint tests and numerical models, particularly under short transient loads. This would ultimately allow improving component-based methods with dynamic properties and enable simplified approaches to progressive collapse arrest of structures.

Hence, development of a tool capable of establishing the non-linear behaviour of T-stubs under short transient loading, once its geometry is provided, would be of use to structural engineers in studying alternative unloading paths capabilities of structures.

REFERENCES

(Abaqus, 2011) Karlsson, & Sorensen, I. U., (2011). *Abaqus Theory Manual, v.6.11.*

(Anderson, 1995) Anderson, T.L., (1995). *Fracture mechanics: fundamentals and applications.* Boca Raton, FL: CRC Press.

(Arup, 2011) Arup (2011). *Review of international research on structural robustness and disproportionate collapse.* Tech. rep., Deparment for Communities and Local Government.

(Barata *et al.*, 2014a) Barata P., Santiago S., Rodrigues J.P. & Rigueiro C., (2014). Development of an experimental system to apply high rates of loading. *XIV Portuguese Conference on Fracture,* Régua, Portugal, (pp. 123-130).

(Barata *et al.*, 2014b) Barata, P., Santiago, A., Rodrigues, J.P., & Rigueiro, C., 2014, "Experimental behaviour of T-stub component subject to impact loads, EUROSTEEL 2014, Naples, 2014 (submitted).

(Barata *et al.*, 2013) Barata, P., Santiago, S., & Rodrigues, J.P., (June 2013)., Experimental behaviour of t-stub joint component at elevated temperatures. *2º CISLACI, Coimbra, Portugal*, (pp. 345-354).

(Bathe, 1996) Bathe, K., 1996, *Finite element procedures*, Prentice-hall, Inc.

(Bursi & Jaspart, 1998) Bursi, O.S. & Jaspart, J.P., (1998) Basic issues in the finite element simulation of extended end plate connections. Computers & Structures, 1998. 69(3): p. 361-382.

(Chang & Tyas, 2011) Chang, L. H., & Tyas, A., (2011). Numerical simulation of steel bolted beam-column connections subjected to dynamic loading. *Applied Mechanics and Materials, 82*, 314-319.

(Cormie & Smith, 2009) Cormie, D. M., & Smith, P., (2009). *Blast Effects on Buildings, 2nd edition.* Thomas Telford.

(Cowper & Symonds, 1957) Cowper, G. R. & Symonds, P. S., (1957). *Strain hardening and strain-rate effects in the impact loading of cantilever beams.* Tech. rep., Brown University Division of Applied Mathematics.

(Daryan & Sadrnejad, 2011) Daryan, A. S. & Sadrnejad, S. A. (2011). The behavior of top and seat bolted angle connections under blast loading. *Journal of Constructional Steel Reaseach, 67*, 1463-1474.

(Dias da Silva, 2006) Dias da Silva, V., (2006). *Mechanics and Strength of Materials.* s.l.:Springer-Verlag.

(Ellingwood, 2007) Ellingwood, B. S. (2007). *Best Practices for Reducing the Potential for Progressive Collapse in Buildings.* NISTIR 7396.

(EN 1991-1-7, 2006) EN 1991-1-7, (2006). Eurocode 1: Actions on structures. Part 1-7, General actions - Accidental actions. Brussels: European Committee for Standardization

(EN 1993-1-8, 2005) EN 1993-1-8, (2005). Eurocode 3: Design of steel structures Part 1-8: Design of joints. Brussels: European Committee for Standardization

(EN 1993-1-10, 2005) EN 1993-1-10, (2005). Eurocode 3: Design of steel structures Part 1-10: Material toughness and through-thickness properties. Brussels: European Committee for Standardization.

(EN10002-1, 2001) EN10002-1, (2001). Metallic – Tensile testing Part 1: Method of test at ambient temperature, Brussels: European Committee for Standardization.

(Faella *et. al.,* 2000) Faella, C., Piluso, V. & Rizzano, G., Structural Steel Semi-Rigid Connections. Boca Raton: CRC Press, 2000.

(Girão Coelho & Simões da Silva, 2004) Girão Coelho, A. B., & Simões da Silva, L. (2004). Experimental assessment of the behaviour of bolted T-stub connections made up of welded plates. *Journal of Constructional Steel Research, 60*, 269-311.

(Girão Coelho, 2004) Girão Coelho, A., (2004).Characterization of the ductility of bolted end plate beam-to-column steel connections, Ph.D. dissertation, Univ. of Coimbra, Coimbra, Portugal

(Girao Coelho, 2013) Girão, A., (2013). "Rotation capacity of partial strength steel joints with three-dimensional finite element approach", Computers and Structures, vol. 116, pp. 88-97

(Hilber *et. al.,* 1977) Hilber, H.M., Hughes., T.J.R. & Taylor, R.L., (1977). Improved numerical dissipation for time integration algorithms in structural dynamics. *Earthquake engineering and structural dynamics, 5*, 283-292.

(Hooputra *et. al.*, 2004) Hooputra, H., Gese, H., Dell, H., & Werner, H., (2004). A comprehensive Failure Model for Crashworthiness Simulation of Aluminium Extrusions. *International Journal of Crashworthiness, 9(5)*, 449-464.

(Hu *et. al.*, 2012) Hu, J. W., Leon, R.T & Park, T., (2012). Mechanical modelling of bolted T-stub connections under cyclic loads, Journal of Constructional Steel Research, Vol. 78, pp. 45-57, 2012.

(Hutton, 2004) Hutton, D. V., (2004) *Fundamentals of Finite Element Analysis*, McGraw-Hill.

(Jaspart, 1991) Jaspart, J., (1991). *Etude de la semi-rigidité des noeuds poutre-colonne et son influence sur la resistance des ossatures en acier.* Ph.D. dissertation, University of Liége, Belgium.

(Johnson & Cook, 1983) Johnson, G.R. & Cook, W.H., (1983). A constitutive model and data for metals subjected to large strains, high strain rates and high temperatures. *Proceedings of the 7th International Symposium on Ballistics, The Hague, The Netherlands*, (pp. 541-547).

(Lemaitre, 1992) Lemaitre, J., (1992). *A course on damage mechanics.* Berlin/Heidelberg: Springer-Verlag.

(Lemaitre, 2001) Lemaitre, J., (2001). Handbook of Materials Behaviour Models, Vol. I, Deformations of Materials, Academic Press

(Malvar & Crawford, 1998) Malvar, L. & Crawford, J., (1998). *Dynamic increase factors for steel reinforcing bars.* Orlando, Florida, In Twenty-eighth department of defence explosives safety board (DDESB) seminar.

(Martins, 2012) Martins, D., (2012). *Variação das propriedades mecânicas do aço com a temperatura, Tese Mestrado,* Portugal: University of Coimbra.

(McAllister, 2002) McAllister, T., (2002). *World Trade Center building performance study: data collection, preliminary observations and recommendations*. Federal Emergency Management Agency, Federal Insurance and Mitigation Administration,Washington, D.C.

(Newmark, 1959) Newmark, N.M., (1959). A Method of computation for structural dynamics, Journal of the Engineering Mechanics Division, Procedings of the ASCE, pp. 67-94.

(Pilluso & Rizzano, 2008) Piluso, V. & Rizzano, G., (2008). Experimental analysis and modelling of bolted T-stubs under cyclic loads, Journal of Constructional Steel Research, vol. 64, 2008, pp.655-669.

(Sabuwala & Krauthammer, 2005) Sabuwala, T. L., & Krauthammer, T., (2005). Finite element analysis of steel beam to column connections subjected to blast loads. *International Journal of Impact Engineering, 31*, 861-876.

(Santiago *et al.*, 2008) Santiago, A., Simões da Silva, L. & Vila Real, P., (2008). Experimental investigation of the behaviour of a steel sub-frame under a natural fire. *International Journal of Steel and Composite Structures, 8(3)*, 243-264.

(Saraiva, 2012) Saraiva, E., (2012). *Variação das propriedades mecânicas do aço relacionadas com problemas de impacto em estruturas*. Master's thesis, Master Thesis at University of Coimbra.

(Simões da Silva *et al.*, 2002) Simões da Silva, L., Santiago. A. & Vila Real, P., (2002). Post-limit Stiffness and Ductility of End-plate Beam-to-column Steel Joints. *Journal Computers and Structures, 80*, 515-531.

(Simões da Silva, 2008) Simões da Silva, L.,(2008). Towards a consistant design approach for steel joints under generalized loading. *Journal of Constructional Steel Research, 64*, 1059-1075.

(Spyrou, 2002) Spyrou, S., (2002). Development of a component-based model of steel beam-to-column joints at elevated temperatures. Ph.D. thesis. University of Sheffield; 2002.

(Stoddart, 2012) Stoddart, E.P., (2012). *Development of component-based connection modelling for steel framed structures subjected to blast or progressive collapse*. Ph.D. dissertation, Faculty of Engineering and the Environment, University of Southampton.

(Stoddart & Tyas 2013) Stoddart, E.P. & Tyas, A, (2013). Strain rate dependent component based connection modelling for use in non-linear dynamic progressive collapse analysis. *Engineering Structures, 55*, 35-43.

(Sun, 2006) Sun, E. Q., (2006). Shear locking and hourglassing in MSC Nastran, ABAQUS, and ANSYS., MSC Software

(Swanson & Leon, 2002) Swanson, J.D. & Leon, R., (2002). Advanced finite element modeling of bolted T-stub connection components. *Journal of Constructional Steel Research, 58 (5-8)*, 1015-1031.

(Szuladziński, 2010) Szuladziński, G., (2010). *Formulas for Mechanical and Structural Shock and Impact*, Boca Raton, FL: CRC Press.

(TM5-1300, 1991) TM 5-1300 - Structures to resist the effects of accidental explosions. (1991). *TM 5-1300 - Structures to resist the effects of accidental explosions*. – **Currently replaced by:** (UFC 3-340-02, 2008) UFC 3-340-02, (2008), Structures to resist the effects of accidental explosions.

(Tyas *et al.*, 2012) Tyas, A., Warren, J.A., Stoddart, E.P., Davison, J.B., Tait, S.J. & Huang, Y., (2012). A methodology for combined rotation-extension testing of simple beam to column joints at high rates of loading, Experimental Mechanics, vol.52, 2012, pp. 1097-1109

(Urgessa & Arciszewski, 2011) Urgessa, G.S. & Arciszewski, T., (2011). Blast response comparison of multiple steel frame connections. Finite Elements in Analysis and Design, 2011. 47(7): p. 668-675.

(Vegte & Makino, 2004) Vegte, G. J. v. d. and Makino, Y., (2004). Numerical simulations of bolted connections: the implicit versus explicit approach. Connections in Steel Structures V. Amsterdam, Netherlands, pp.89-94, 2005.

(Xu & Ellingwood, 2011) Xu, G. & Ellingwood, B.R., (2011). Disproportionate collapse performance of partially restrained steel frames with bolted T-stub connections, Engineering Structures, vol. 33, 2011, pp. 32-43

(Yang & Tan, 2012) Yang, B. & Tan, K.H., (2012). Numerical analyses of steel beam–column joints subjected to catenary action. Journal of Constructional Steel Research, 2012. **70**(0): p. 1-11.

(Yim & Krauthammer, 2009) Yim, H. C., & Krauthammer, T., (2009). Load impulse characterization for steel connection. *International Journal of Impact Engineering, 36*, pp….. 737-745.

(Yu *et al.*, 2009) Yu H., Burgess, I.W., Davison, J.B. and Plank, R.J., (2009). Development of a yield-line model for endplate connections in fire, Journal of Constructional Steel Research, Vol. 65, pp. 1279-1289

(Zoetemeijer, 1974) Zoetemeijer, P., (1974). A design method for the tension side of statically-loaded, bolted beam-to-column joints. *Heron, 20(1)*, 1-59.

(Fukui – Earthquake, 1948) http://commons.wikimedia.org/wiki/File:Fukui_Earthquake_1948_-_damaged_building.jpg

(Windsor Tower, Madrid – Fire, 2005) http://commons.wikimedia.org/wiki/File:Ruins_of_Torre_Windsor,_Madrid_2.JPG

(Ronan point, London – accidental gas explosion, 1968) http://en.wikipedia.org/wiki/Ronan_Point

APPENDICES

Appendix A – List of publications

Journal manuscript submitted for publication:

- **Fire Safety Journal**

Barata, P., Ribeiro, J., Rigueiro, C., Santiago,A., Rodrigues, J.P., "*Assessment of t-stub joint component at ambient and elevated temperatures*", Fire Safety Journal. (accepted with revisions)

- **International Journal of Impact Engineering**

Ribeiro J., Santiago A., Rigueiro M.C. and Veljkovic, M., " *Numerical assessment of T-stub component subject to impact loading*", International Journal of Impact Engineering. (accepted with revisions)

- **Journal of Constructional Steel Research**

Ribeiro J., Rigueiro M.C., Santiago A., Simões da Silva, L., "*An analytical model for the response of t-stub component under impact loading*", Journal of Constructional Steel Research. (submitted)

- **International Journal of Structural Integrity – PCF 2014 Special Edition**

Ribeiro J., and Santiago, A. and Rigueiro, M.C., "*Material modelling of tensile steel component under impulsive loading*", International Journal of Structural Integrity – PCF 2014 Special Edition (submitted)

National conference participation with oral presentation:

Ribeiro, J., Rigueiro, C., Santiago, A., "*Análise Dinâmica Não Linear De Ligações Viga-Pilar Aparafusadas Com Placa De Extremidade*", IX CMM, Congresso de Construção Metálica e Mista, pp. 337-346, Porto, Portugal, 24 – 25 October 2013.

- Link:http://isise/smct/private/index.php?process=download&id=3041&code=7d5c15ad14829cf1ce5850f269e87b4be9ea8ab1

Ribeiro, J., Santiago, A., Rigueiro, C., "*Material modelling of tensile steel component under impulsive loading*", XIV Portuguese Conference on Fracture, pp. 273-280, Régua, Portugal, February 2014

- Link:http://isise/smct/private/index.php?process=download&id=4928&code=ILu7ioKn

International conference participation with oral presentation:

Ribeiro J., Rigueiro C. and Santiago A., "*Numerical behaviour of T-stub joint component at ambient and elevated temperatures*", Vol. I, pp. 355-364, in 2º CISLACI 2013: Coimbra, 2013.

- Link:http://isise/smct/private/index.php?process=download&id=3038&code=c422202d2d2863d58ec1d04ca37deccef3fed58e

Ribeiro, J., Rigueiro, C., Santiago, A., "*Post-impact fire resistance of T-stub joint component: numerical evaluation*", ASFE 2013, Conference: Applications of Structural Fire Engineering, Prague, Czech Republic, 19-20 April 2013

- Link:http://isise/smct/private/index.php?process=download&id=3039&code=18df4bbd46cabde9ba9f41c447ba97df93a851e1

Ribeiro, J., Rigueiro, C., Santiago, A., "*Numerical assessment of T-stub component subjected to impact loading*", CMN 2013, Congreso de Métodos Numéricos en Ingeniería, Bilbao, Spain, 25 – 28 June 2013.

- Link:http://isise/smct/private/index.php?process=download&id=3040&code=c97257125ae0ca7c515f9ae28e7e8a8f5d35eeb8

Ribeiro, J., Santiago, A., Rigueiro, C., Assessment of the t-stub component subject to high strain-rate, EURODYN 2014, Porto, Portugal, July 2014.

- Link:http://isise/smct/private/index.php?process=download&id=4931&code=jOeFhpsV

❖ **COST ACTION IFER TU0904 - Application of Structural Fire Design**

Ribeiro J., Santiago A. e Rigueiro M.C., "Post-impact fire resistance of t-stub joint component: numerical evaluation"; COST ACTION IFER TU0904 - Application of Structural Fire Design; pp. 242-249, Prague, Czech Republic, 19-20 April 2013.

Conference participation accepted for oral presentation:

Ribeiro J., Rigueiro M.C. and Santiago A., "*Numerical validation of T-stub component subject to impact load*", EUROSTEEL 2014, Naples, September, 2014.

Appendix B – Reference guide & Workflow

Literature inputs:

Structural behaviour:

(Arup, 2011)

(Cormie & Smith, 2009)

(Ellingwood, 2007)

(EN 1991-1-7, 2006)

Connection behaviour:

(EN 1993-1-8, 2005)

(Faella *et. al.,* 2000)

(Girao Coelho, 2013)

(Simões da Silva *et al.*, 2002)

(Simões da Silva, 2008)

T-stub response:

(EN 1993-1-8, 2005)

(Faella *et. al.,* 2000)

(Girão Coelho & Simões da Silva, 2004)

(Girão Coelho, 2004)

(Swanson & Leon, 2002)

Analytical models:

(Faella *et. al.,* 2000)

(Spyrou, 2002)

(Zoetemeijer, 1974)

(Yu *et al.*, 2009)

Finite Element Method:

(Hilber *et. al.,* 1977)

(Bathe, 1996)

(Hutton, 2004)

(Vegte & Makino, 2004)

(Abaqus, 2011)

ImpactFIRE inputs:

Material characterization:

(Saraiva, 2012)

(Martins, 2012)

Testing setup:

(Barata *et al.*, 2014a)

Material Modelling:

Hardening:

(Lemaitre, 2001)

(Dias da Silva, 2006)

Viscoplasticity:

(Cowper & Symonds, 1957)

(Johnson & Cook, 1983)

(Malvar & Crawford, 1998)

Damage:

(Lemaitre, 1992)

(Anderson, 1995)

(Hooputra *et. al.*, 2004)

Short transient & blast loading:

(TM5-1300, 1991)

(Yim & Krauthammer, 2009)

(Chang & Tyas, 2011)

(Daryan & Sadrnejad, 2011)

(Urgessa & Arciszewski, 2011)

(Stoddart, 2012)

(Tyas *et al.*, 2012)

(Stoddart & Tyas 2013)

T-stub test under static loading:

(Barata *et al.,* 2013)

T-stub test under impact loading:

(Barata *et al.,* 2014b)

MSc. Thesis

T-stub component under impact loading

João Ribeiro

i. Finite Element Model – T-stub component under impact loads;
ii. Validation (Static & Dynamic) & Parametric studies;
   a. Load magnitude;
   b. Load application time;
   c. T-stub thickness.
iii. Analytical models
   a. Study and proposal to include material dynamic properties.

Appendix C – Strain rate laws

Cowper-Symonds

Rate dependent plasticity model proposed by Cowper and Symonds, (Cowper & Symonds, 1957) follows the equation:

$$\sigma_{dyn}/\sigma_{static} = 1 + \left(\frac{\dot{\varepsilon}^{pl}}{\gamma}\right)^{m}$$

where σ_{yd} is the dynamic yield strain; $\dot{\varepsilon}^{pl}$ is the equivalent plastic strain rate; γ is the viscosity parameter and m is the strain rate hardening parameter. The suggested values for mild steel are γ = 40 s^{-1} and m = 0.2.

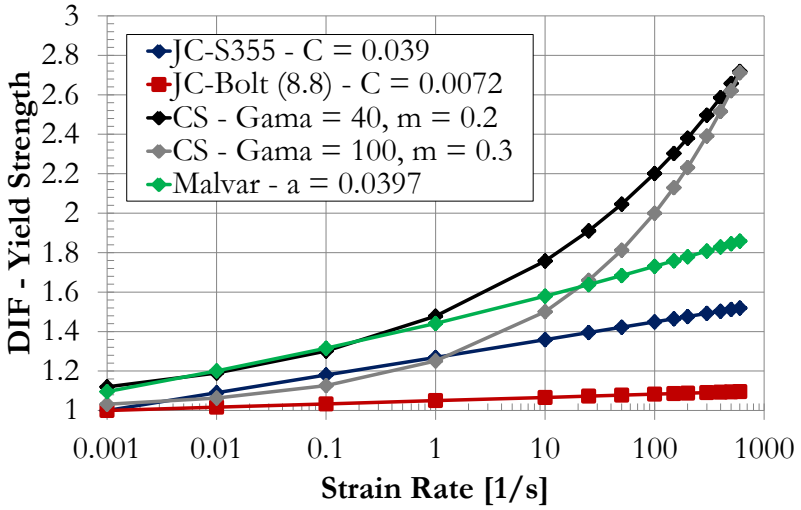

Appendix Fig. I – Comparison of the different strain rate description law's; JC – Johnson-Cook; CS – Cowper Symonds

The Cowper-Symonds law in grey, attempts to deliverer the values obtained with the Johnson-Cook law, in blue (used in the numerical models presented), through calibration of γ and m.

Malvar-Crawford

Malvar and Crawford (Malvar & Crawford, 1998) have conducted dynamic tests on rebar specimens of grades 40, 60 and 75 in order to assess the behaviour of concrete structures

subject to blast loads. They found the elastic modulus and that ultimate strain (at peak stress) to remain constant under dynamic loading when compared to static values, however they assume different DIF values for the elastic and ultimate strength. The formulation is valid for bars with yield stresses between 290 and 710 MPa and for strain rates between 10^{-4} and 225 s^{-1}. It demonstrates that for higher strength steel the effects are minor.

$$DIF = \left(\frac{\dot{\varepsilon}}{10^{-4}}\right)^{\alpha}$$

Where: $\alpha_{fy} = 0.074 - 0.040\frac{f_y}{414}$

and $\dot{\varepsilon}$ is the strain rate $[s^{-1}]$ and f_y the yield strength [MPa].

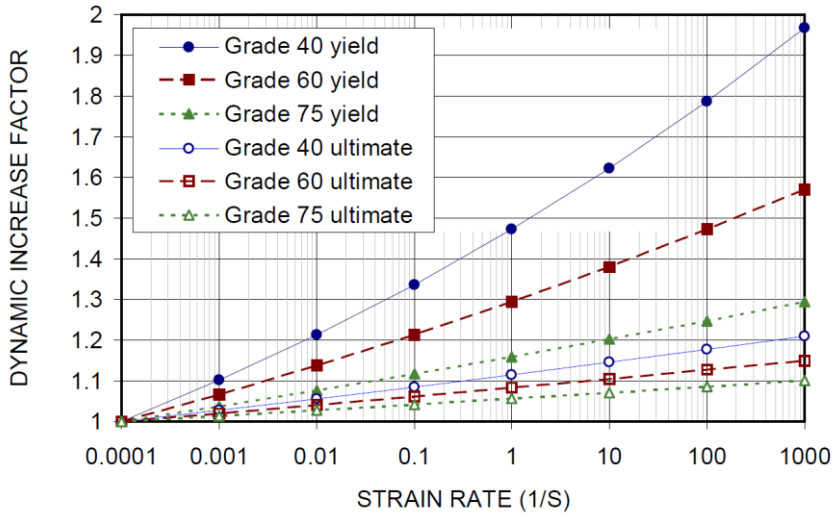

Appendix Fig. II – Proposed DIF for ASTM A615 Grade 40, 60, 7 steel rebar (Malvar & Crawford, 1998)

UFC 3-340-02 (replacing TM5-1300)

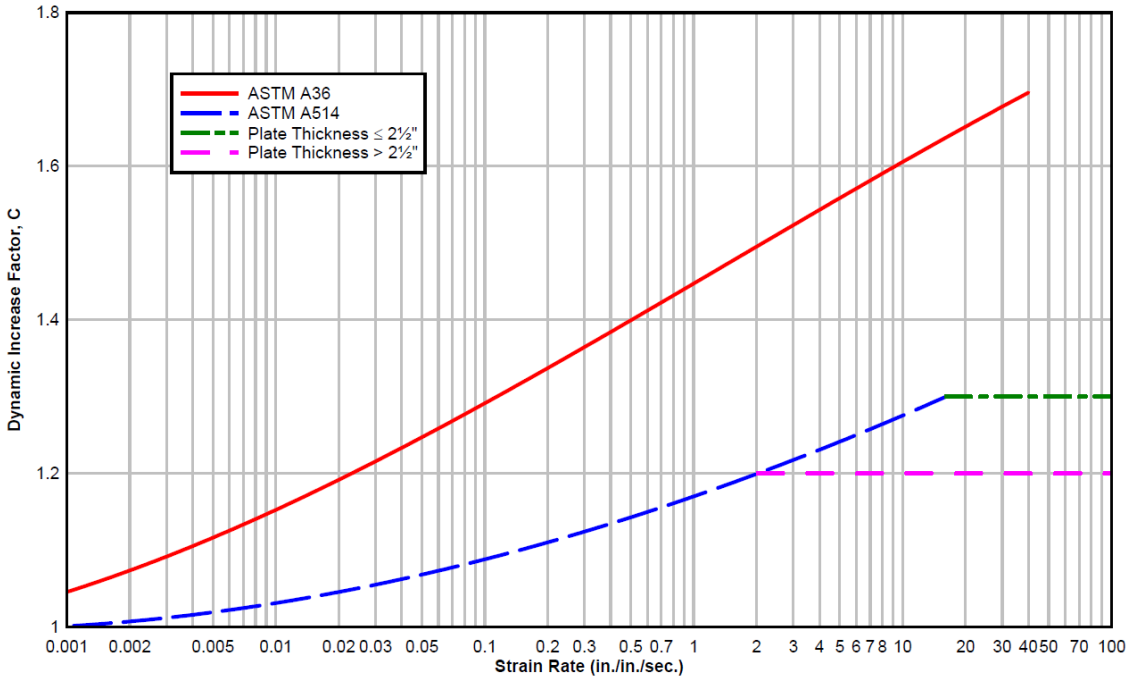

Appendix Fig. III – DIF for yield stress at various strain rates for ASTM A-36 and A-514 steels (UFC 3-340-02, 2008)

Appendix D – Main Tools

MS Word – text writing;

MS Excel – spreadsheet calculation;

Visual Basic – programming language for macro development

ABAQUS – general purpose finite element software;

Python – open-source programming language for scripting;

Sketchup – Computer assisted drawing tool;

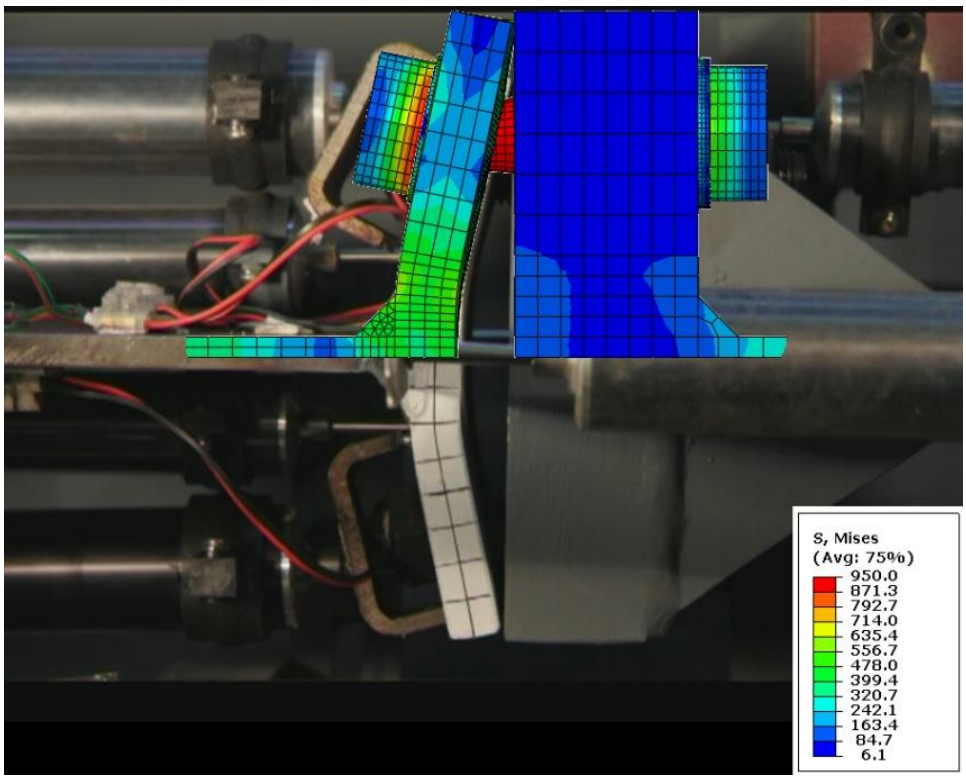

Assessment of the behaviour of T-stub joint under impact loading

João Nuno Bregieiro Ribeiro

UC 2003 105316

E-mail: jnribeiro@gmail.com

Coimbra, July 2014